

# Terrestrial Planet Formation I. The Transition from Oligarchic Growth to Chaotic Growth<sup>1</sup>

Scott J. Kenyon

*Smithsonian Astrophysical Observatory, 60 Garden Street, Cambridge, MA 02138, USA;  
e-mail: skenyon@cfa.harvard.edu*

and

Benjamin C. Bromley

*Department of Physics, University of Utah, 201 JFB, Salt Lake City, UT 84112, USA;  
e-mail: bromley@physics.utah.edu*

## ABSTRACT

We use a hybrid, multiannulus,  $n$ -body-coagulation code to investigate the growth of km-sized planetesimals at 0.4–2 AU around a solar-type star. After a short runaway growth phase, protoplanets with masses of  $\sim 10^{26}$  g and larger form throughout the grid. When (i) the mass in these ‘oligarchs’ is roughly comparable to the mass in planetesimals and (ii) the surface density in oligarchs exceeds  $2\text{--}3\text{ g cm}^{-2}$  at 1 AU, strong dynamical interactions among oligarchs produce a high merger rate which leads to the formation of several terrestrial planets. In disks with lower surface density, milder interactions produce several lower mass planets. In all disks, the planet formation timescale is  $\sim 10\text{--}100$  Myr, similar to estimates derived from the cratering record and radiometric data.

*Subject headings:* planetary systems – solar system: formation – stars: formation – circumstellar matter

## 1. INTRODUCTION

In the protosolar nebula, the growth of terrestrial planets begins with collisions and mergers of planetesimals, solid objects with radii of  $\sim 1$  km (e.g. Safronov 1969; Lissauer

---

<sup>1</sup>Calculations reported here used the ‘hydra’ cluster run by the Computation Facility of the Harvard-Smithsonian Center for Astrophysics

1987; Wetherill & Stewart 1993; Weidenschilling et al. 1997). Initially, planetesimals grow slowly. As they grow, dynamical friction circularizes the orbits of the largest objects; viscous stirring excites the orbits of the smallest objects. Slow, orderly growth ends when the gravitational cross-sections of the largest objects exceed their geometric cross-sections. Because dynamical friction is faster than accretion, the largest objects stay on circular orbits and grow faster and faster relative to the smallest planetesimals. This runaway growth rapidly concentrates solid material into a few protoplanets (e.g., Greenberg et al. 1978; Greenberg et al. 1984; Wetherill & Stewart 1989, 1993; Weidenschilling et al. 1997; Kenyon & Luu 1998; Kokubo & Ida 2000).

During runaway growth, protoplanets stir the orbits of the leftover planetesimals. Stirring reduces gravitational focusing factors and slows the growth of the protoplanets (Wetherill & Stewart 1993; Ida & Makino 1993; Kenyon & Bromley 2002; Rafikov 2003c). Although protoplanets grow slowly, they grow faster than the leftover planetesimals and intermediate mass objects do. These large ‘oligarchs’ slowly clear their orbits of smaller objects and reach a maximum ‘isolation mass’ that depends on the initial surface density of solid material (Lissauer 1987; Lissauer & Stewart 1993; Kokubo & Ida 1998; Rafikov 2003c; Goldreich, Lithwick & Sari 2004b).

Throughout oligarchic growth, protoplanets repel other oligarchs in the disk (Kokubo & Ida 1996, 1998, 2000; Kominami & Ida 2002; Thommes, Duncan, & Levison 2003). Eventually, however, dynamical interactions produce collisions and gravitational scattering among the oligarchs (Chambers 2001; Kokubo & Ida 2002; Kominami & Ida 2002; Thommes, Duncan, & Levison 2002; Rafikov 2003c; Goldreich, Lithwick & Sari 2004b). During this phase of ‘chaotic growth’, the largest oligarchs merge with and clear away other oligarchs and smaller objects to become full-fledged planets (e.g., Goldreich, Lithwick & Sari 2004a).

Within this framework, the transition from oligarchic growth to chaotic growth is poorly understood. Although analytic estimates provide a guide to the late evolutionary stages (e.g., Rafikov 2003c; Goldreich, Lithwick & Sari 2004a), numerical calculations are necessary to test the basic theory and to derive the end states and timescales as a function of initial conditions (e.g. Kominami & Ida 2002). Published calculations do not test this regime of the theory in much detail. Pure coagulation and simple hybrid calculations cannot follow the transition accurately (Wetherill & Stewart 1993; Weidenschilling et al. 1997). Direct  $n$ -body calculations with planetesimals are computationally expensive and tend to focus on evolution during oligarchic growth, when orbits of individual objects are easier to track (Alexander & Agnor 1998; Kokubo & Ida 2002, and references therein). Direct  $n$ -body calculations without planetesimals follow dynamical interactions after the transition and

concentrate on the clearing phase (Chambers 2001). Thus, understanding this evolutionary phase requires new calculations (see the discussion in Kokubo & Ida 2002).

Here, we use numerical calculations with a new hybrid  $n$ -body-coagulation code to investigate the transition from oligarchic growth to chaotic growth. Our approach allows us to combine statistical algorithms for the planetesimals with direct  $n$ -body integrations of the oligarchs. From several simple test cases and complete planet formation calculations, we show that oligarchic growth becomes chaotic when the orbits of oligarchs begin to overlap. If the surface density in oligarchs exceeds a critical value, this transition occurs when the oligarchs contain roughly half of the mass in solids. At 1 AU, the critical initial surface density is  $\Sigma_c \approx 2\text{--}3 \text{ g cm}^{-2}$ . Thus, oligarchs can make the transition from oligarchic to chaotic growth in disks with masses comparable to the minimum mass solar nebula, where  $\Sigma \approx 8\text{--}10 \text{ g cm}^{-2}$  at 1 AU.

In disks where the surface density of solids is below the limit for chaotic growth, oligarchs slowly merge to form larger objects. Pairwise interactions, instead of large-scale chaos, drive the dynamics of these systems. Milder, slower interactions between oligarchs then produce less massive planets.

We develop the background for our calculations in §2, describe a suite of calculations in §3, and conclude with a brief summary and conclusions in §4.

## 2. BACKGROUND

The evolution from planetesimals to planets is marked by several phases – orderly growth, runaway growth, oligarchic growth, and chaotic growth – with clear transitions in the dynamics and mutual interactions of the ensemble of solid objects. Analytic derivations and sophisticated coagulation and  $n$ -body calculations identify the physics of these transitions. Here, we summarize some basic results to provide the context for our numerical simulations.

Most considerations of planet formation begin with small objects,  $r_i \lesssim 1 \text{ km}$ , that contain all of the solid material. For these sizes, collisional damping and viscous stirring roughly balance for orbital eccentricity  $e \sim 10^{-5}$ . The gravitational binding energy,  $E_g \sim 10^4 \text{ erg g}^{-1}$ , is then comparable to the typical collision energy at 1 AU,  $E_c \sim 10^3\text{--}10^4 \text{ erg g}^{-1}$ . Both energies are smaller than the disruption energy – the collision energy needed to remove half of the mass from the colliding pair of objects – which is  $Q_d \gtrsim 10^7 \text{ erg g}^{-1}$  for rocky material (Davis et al. 1985; Benz & Asphaug 1999). Thus, collisions produce mergers instead of debris.

Initially, growth from mergers is slow. The collision cross-section is the product of the geometric cross-section and the gravitational focusing factor,

$$\sigma_c \sim \pi r^2 f_g \sim \pi r^2 (1 + \beta (ev_K/v_{esc})^2), \quad (1)$$

where  $r$  is the particle radius,  $v_K$  is the orbital velocity,  $v_{esc}$  is the escape velocity, and  $\beta$  is a coefficient that accounts for three-dimensional orbits in a rotating disk (Greenzweig & Lissauer 1990; Spaute et al. 1991; Wetherill & Stewart 1993). Because  $ev_K \approx v_{esc}$ , gravitational focusing factors are small. Thus, growth is slow and orderly (Safronov 1969).

As larger objects form, the smaller objects effectively damp the orbital eccentricity of larger particles through dynamical friction (e.g. Wetherill & Stewart 1993; Kokubo & Ida 1995; Kenyon & Luu 1998). Viscous stirring by the large objects heats up the orbits of the small objects. In the case where gas drag is negligible, Goldreich, Lithwick & Sari (2004b) derive a simple relation for the ratio of the eccentricities of the large (‘l’) and the small (‘s’) objects in terms of their surface densities  $\Sigma_{l,s}$  (see also Kokubo & Ida 2002; Rafikov 2003a, 2003b, 2003c),

$$\frac{e_l}{e_s} \sim \left( \frac{\Sigma_l}{\Sigma_s} \right)^n, \quad (2)$$

with  $n = 1/4$  to  $1/2$ . For  $\Sigma_l/\Sigma_s \sim 10^{-3}$  to  $10^{-2}$ ,  $e_l/e_s \approx 0.1$ – $0.25$ . Because  $e_s v_K \lesssim v_{l,esc}$ , gravitational focusing factors are large. Runaway growth begins.

Runaway growth concentrates more and more mass in the largest objects. Dynamical friction produces the largest gravitational focusing factors among the largest objects. These protoplanets run away from the smaller objects and contain an ever growing fraction of the total mass. At the same time, the large objects continue to stir the leftover planetesimals. The leftovers have orbital velocity dispersions comparable to the escape velocities of the oligarchs. With  $e_s v_K \sim v_{esc}$ , equations (1) and (2) show that collision rates decline as runaway growth continues. The ensemble of protoplanets and leftover planetesimals then enters the oligarchic phase, where the largest objects grow faster than the leftover planetesimals.

Among the oligarchs, the smaller oligarchs grow the fastest. Each oligarch tries to accrete all of the material in an annular ‘feeding zone’ set by balancing the gravity of neighboring oligarchs. Within each annulus, each oligarch stirs up the remaining planetesimals along its orbit. Because smaller oligarchs orbit in regions with smaller  $\Sigma_l/\Sigma_s$ , equations (1) and (2) show that smaller oligarchs have larger gravitational focusing factors. Thus smaller oligarchs grow faster (e.g., Kokubo & Ida 1998; Goldreich, Lithwick & Sari 2004b).

During oligarchic growth, protoplanets become isolated from their surroundings (Lissauer & Stewart 1993; Kokubo & Ida 1998, 2000; Thommes, Duncan, & Levison 2003;

Goldreich, Lithwick & Sari 2004a,b). As oligarchs accrete smaller planetesimals, dynamical interactions push them apart to maintain a typical separation of 5–10 Hill radii,  $R_H = (m/3m_\odot)^{1/3}$ , where  $m$  is the mass of an oligarch and  $m_\odot$  is the mass of the Sun. The separation depends weakly on the mass and semimajor axis of the protoplanet and the local surface density (Kokubo & Ida 1998, 2000).

Oligarchic growth limits the mass of the largest protoplanets (Lissauer 1987; Lissauer & Stewart 1993; Kokubo & Ida 1998). If an oligarch accretes all planetesimals within a torus of width  $a_{acc} = nR_H$ , it has a mass  $m \approx 0.005\text{--}0.01\ n^{3.2}m_\oplus$ , where  $m_\oplus$  is the mass of the Earth. For  $n \sim 5$ , the so-called isolation mass is  $m_{iso} \sim 0.1\ m_\oplus$ . Unless oligarchs move out of their feeding zones or additional material is brought into the feeding zone, they cannot grow beyond the isolation mass.

A transition from oligarchic growth to chaotic growth appears to provide the best way for oligarchs to evolve into planets (e.g., Kominami & Ida 2002; Goldreich, Lithwick & Sari 2004b). Small oligarchs on roughly circular orbits prevent radial drift by repelling planetesimals and opening up a gap in the feeding zone (Rafikov 2001, 2003a,b,c,d). Larger oligarchs that stir up planetesimals outside the gap can grow up to the isolation mass, but no further (Rafikov 2003c; Goldreich, Lithwick & Sari 2004a,b). Once the mass in the oligarchs exceeds the mass in leftover planetesimals, dynamical interactions between the oligarchs move them outside their feeding zones. The oligarchs then compete for the remaining planetesimals (Goldreich, Lithwick & Sari 2004a,b). Goldreich, Lithwick & Sari (2004a) propose that large-scale dynamical interactions begin when  $\Sigma_l \gtrsim \Sigma_s$ . However, this regime has not been investigated in detail by numerical simulations.

To evaluate the conditions necessary for chaotic orbits to produce terrestrial planets, we calculate the formation of planets from 1–10 km planetesimals. We start with several test calculations to demonstrate and to examine the physical processes involved in oligarchic growth and the transition from oligarchy to chaos. We then consider the growth of planets in a small torus at 0.84–1.16 AU and a large torus at 0.4–2 AU.

To provide a measure of the orbital interactions in the calculations, we define two parameters for the ensemble of oligarchs. From published  $n$ -body calculations, we expect significant orbital interactions between oligarchs when their typical separations are less than 5–10  $R_H$  (Kokubo & Ida 1995, 1998; Thommes, Duncan, & Levison 2003; Bromley & Kenyon 2006). With  $N$  equal mass oligarchs spaced evenly in radial distance within a torus of width  $\Delta a$ , oligarchs should begin to interact when  $5 - 10NR_H \approx \Delta a$ . Generalizing this idea to  $N$  oligarchs of any mass, we expect significant orbital interactions among oligarchs when the sum of their Hill radii is  $\sim 0.1\text{--}0.2\ \Delta a$ . To provide a measure of the onset of

interactions, we define a Hill parameter as the normalized sum of Hill radii for all oligarchs:

$$p_H = \frac{\sum_{i=1}^N R_{H,i}}{a_{out} - a_{in}}, \quad (3)$$

where  $R_{H,i}$  is the Hill radius for each of  $N$  oligarchs and  $a_{in}$  ( $a_{out}$ ) is the inner (outer) radius of the coagulation grid. We expect significant dynamical interactions due to orbit overlap when  $p_H \gtrsim 0.1$ .

The Hill parameter is useful, because we can relate  $p_H$  to the surface density required for overlapping orbits. If  $m_t$  is the typical mass of an oligarch in equation (3), the surface density in oligarchs is roughly

$$\Sigma_l \approx 2.5 \left( \frac{p_H}{0.1} \right) \left( \frac{m_t}{10^{26} \text{ g}} \right)^{2/3} \text{ g cm}^{-2}. \quad (4)$$

If oligarchic growth ends when  $p_H \approx 0.1$ , equation (3) yields  $\Sigma_l \sim 2\text{--}3 \text{ g cm}^{-2}$ , which is 25% to 33% of the mass in a minimum mass solar nebula (Weidenschilling 1977; Hayashi 1981).

To provide a second measure of the transition from oligarchic to chaotic growth, we derive an orbit crossing parameter. We define the absolute value of the difference in the semimajor axis of two oligarchs,  $a_{sep,ij} = |a_i - a_j|$ . For each oligarch with  $j \neq i$ , we evaluate  $x_{ij} = (a_{sep} - a_j e_j) / R_{H,ij}$ , where  $e_j$  is the orbital eccentricity and

$$R_{H,ij} = \left( \frac{m_i + m_j}{3m_\odot} \right)^{1/3} \left( \frac{a_i + a_j}{2} \right) \quad (5)$$

is the mutual Hill radius. We find the minimum value of  $x_{ij}$ ,  $x_{min,i} = \min(x_{ij})$ . The orbit crossing parameter is then

$$p_o = \frac{\sum_{i=1}^N m_i x_{min,i}}{m_{tot}}, \quad (6)$$

where  $m_{tot}$  is the total mass in oligarchs. When  $p_o \gtrsim 5$ , the orbits of oligarchs do not cross. When  $p_o \sim 0$ , most orbits cross. We expect significant orbital interactions, mergers, and chaotic growth when  $p_o \lesssim 0$ .

### 3. NUMERICAL CALCULATIONS

#### 3.1. Methods

To explore the end of oligarchic growth, we consider numerical calculations of planet formation. Because the initial number of planetesimals is large,  $\sim 10^8$  to  $10^9$ , a statistical

approach is the only plausible method to derive the collisional growth of planetesimals (e.g. Safronov 1969; Wetherill & Stewart 1993). When a few objects contain most of the mass, the statistical approach fails. N-body methods can then treat the behavior of the largest objects but cannot follow the evolution of the leftover planetesimals. Here, we use a hybrid n-body-coagulation code, which combines the statistical and n-body approaches to follow the growth of 1–10 km planetesimals into planets.

Kenyon & Bromley (2004a, and references therein) summarize our multi-annulus coagulation code. The model grid contains  $N$  concentric annuli with widths  $\delta a_i$  centered at heliocentric distances  $a_i$ . Each annulus contains  $n(m_{ik}, t)$  objects of mass  $m_{ik}$  with orbital eccentricity  $e_{ik}(t)$  and inclination  $i_{ik}(t)$  in  $M$  mass batches. Our solution of the coagulation and Fokker-Planck equations treats elastic and inelastic collisions between all particles in all annuli. We adopt collision rates from kinetic theory – the particle-in-a-box method – and use an energy-scaling algorithm to assign collision outcomes. We derive changes in orbital parameters from gas drag, dynamical friction, and viscous stirring (Adachi et al. 1976; Ohtsuki, Stewart, & Ida 2002).

Bromley & Kenyon (2006) describe the n-body code and our methods for combining n-body calculations with the coagulation code. When an object in the coagulation code reaches a preset mass, it is ‘promoted’ into the n-body code. To set the initial orbit for this object, we use the three coagulation coordinates,  $a$ ,  $e$ , and  $i$ , and select random values for the longitude of periastron and the argument of perihelion. Because the annuli have finite width  $\delta a_i$ , where  $i$  is the index, we set the semimajor axis of the promoted object to  $a_p = a_i + (0.5 - x)\delta a_i$ , where  $x$  is a random number between 0 and 1. When two or more objects within an annulus are promoted to the n-body code during the same timestep, we restrict the choices of the orbital elements to minimize orbital interactions between the newly promoted  $n$ -bodies.

We follow the mutual interactions of the ensemble of ‘n-bodies’, including mergers, using a robust set of integrators. These integrators include accretion and drag terms that link the evolution of the planetesimals to the evolution of the n-bodies. To compute how rapidly n-bodies accrete planetesimals, we adopt a particle-in-a-box formalism. Direct calculations for gas drag and Fokker-Planck gravitational interactions provide rates for changes in  $a$ ,  $e$ , and  $i$  for each n-body due to interactions with planetesimals.

Bromley & Kenyon (2006) describe tests of the hybrid code along with initial results for terrestrial planet formation. When the Hill radius of a promoted n-body is small compared to the separation of annuli in the coagulation grid, the hybrid code reproduces published results of previous investigations (e.g. Greenzweig & Lissauer 1990; Wetherill & Stewart 1993; Weidenschilling et al. 1997; Duncan, Levison & Lee 1998; Chambers 2001). In the

calculations described below, we set the promotion mass to  $m_{pro} = 1\text{--}30 \times 10^{24}$  g, which yields a small Hill radius,  $\sim 0.0005\text{--}0.002$   $a$ , compared to the separation of adjacent annuli in the coagulation grid,  $\sim 0.01\text{--}0.04$   $a$ .

Our numerical calculations begin with a mass distribution of planetesimals in 32–64 concentric annuli with initial surface density  $\Sigma = \Sigma_0 (a/1 \text{ AU})^n$ , with  $n = 1\text{--}1.5$ . The spacing between successive mass batches is  $\delta = m_{i+1}/m_i$ . We adopt  $\delta = 1.4\text{--}2.0$  for most calculations. All planetesimals start with initial eccentricity  $e_0$  and inclination  $i_0$ . As planetesimals evolve, the average mass  $m_{ik}$  and orbital parameters  $e_{ik}$  and  $i_{ik}$  of each mass batch change. We add mass batches as planetesimals grow in mass and reserve 8–16 mass batches in each annulus for n-bodies. Throughout the calculation, gas drag and collisions transport planetesimals in the coagulation code from one annulus to another. In addition to these processes, mutual gravitational interactions can scatter n-bodies into different annuli.

For these calculations, we assume a simple treatment of the gas. The midplane density is

$$\rho_g(a, t) = \rho_0(a) e^{-t/t_0}, \quad (7)$$

where  $\rho_0(a)$  is the initial gas density and  $t_0$  is a constant. We adopt a gas surface density  $\Sigma_g = 100\Sigma$  and set  $\rho_0 = \Sigma_g/2H$ , where  $H$  is the gas scale height (Kenyon & Hartmann 1987). Consistent with observations of pre-main sequence stars, we adopt  $t_0 = 1$  Myr (see, for example, Haisch, Lada, & Lada 2001; Young et al. 2004; Calvet et al. 2005; D’Alessio et al. 2005).

### 3.2. Simple model

To isolate the important physical parameters in the evolution of oligarchs, we first consider an ensemble of equal mass planetesimals in 32 concentric annuli at 0.84–1.16 AU. The planetesimals have mass  $m_s$ , surface density  $\Sigma = \Sigma_s(a/1 \text{ AU})^{-3/2}$ , initial eccentricity  $e_0 = 10^{-5}$  and inclination  $i_0 = e_0/2$ . Within this swarm, we embed  $N$  oligarchs with mass  $m_l$  and surface density  $\Sigma = \Sigma_l(a/1 \text{ AU})^{-3/2}$ . The oligarchs have the same initial eccentricity and inclination as the planetesimals.

To evolve this ensemble in time, we calculate gravitational stirring for all interactions. We allow oligarchs – but not planetesimals – to collide and merge. This assumption allows us to focus on the dynamical evolution of the oligarchs in the absence of planetesimal accretion.

Figure 1 shows the evolution of the eccentricity for three sets of oligarchs with  $\Sigma_l/\Sigma_s = 0.5$  and  $\Sigma_l = 1\text{--}4 \text{ g cm}^{-2}$ . The planetesimals have  $m_s = 10^{24}$  g; the oligarchs have  $m_l = 10^{26}$  g, comparable to the isolation mass for this grid. The Hill parameter increases from  $p_H = 0.04$



(lower panel) to  $p_H = 0.07$  (middle panel) to  $p_H = 0.13$  (upper panel). In each frame, the colored tracks indicate the eccentricities of oligarchs in the grid. Along the track of a single oligarch, the color changes when two oligarchs merge. Although a single color does not track the motion of an individual oligarch throughout the evolution, the ensemble of curves tracks the merger history of the final set of oligarchs. Tracking backwards in time along connected curves yields the evolution of one of the oligarchs that remains at the end of the calculation. The legends list  $\Sigma_l$  and the initial and final number of oligarchs (Figure 2).

The eccentricity evolution is sensitive to the initial mass in the swarm. For  $\Sigma_l = 1 \text{ g cm}^{-2}$ , the oligarchs have a typical separation of 15–20  $R_H$  and do not have significant interactions. As the oligarchs stir up the planetesimals, dynamical friction maintains a constant ratio  $e_s/e_l \sim (m_l/m_s)^{1/2} \sim 0.1$ . Although the orbits of the oligarchs become more and more eccentric, the growth of  $e_l$  is slow (Figure 1, lower panel). It takes  $\sim 1 \text{ Myr}$  to reach  $e_l \sim 0.01$  and another 8–9 Myr to reach  $e_l \sim 0.02$ . After  $\sim 100 \text{ Myr}$ , when  $e \sim 0.04$ , the orbits begin to overlap.

As  $\Sigma_l$  increases, orbital interactions occur on shorter timescales (Figure 1, middle and upper panels). For  $\Sigma_l = 2 \text{ g cm}^{-2}$ , the initial separation of the oligarchs is  $\sim 10\text{--}12 \text{ } R_H$ . It takes only  $5 \times 10^4 \text{ yr}$  for the typical eccentricity to reach  $e \sim 0.01$ , when the minimum separation between oligarchs is only  $\sim 8 \text{ } R_H$ . At  $\sim 10^5 \text{ yr}$ ,  $e \sim 0.02$  and orbits overlap. Two oligarchs merge at  $\sim 2 \times 10^5 \text{ yr}$ ; two more merge at  $\sim 1 \text{ Myr}$ . When we stop the calculation at 1 Myr, two oligarchs remain in eccentric orbits,  $e \gtrsim 0.025$  and are likely to merge with other oligarchs.

For  $\Sigma_l = 4 \text{ g cm}^{-2}$ , orbits begin to overlap in  $\sim 10^4 \text{ yr}$ . After a single merger at  $\sim 10^4 \text{ yr}$ , orbits continue to grow more eccentric. At  $5 \times 10^4 \text{ yr}$ , all orbits overlap and the merger rate accelerates. There are two additional mergers at  $\sim 10^5 \text{ yr}$ , another two by  $3 \times 10^5 \text{ yr}$ , and three more by  $\sim 1 \text{ Myr}$ . At 1 Myr, all of the remaining oligarchs have eccentric, overlapping orbits and many are likely to merge over the next few Myr.

Figure 2 illustrates the chaotic behavior of the semimajor axis in these test cases. For  $\Sigma_l = 1 \text{ g cm}^{-2}$ , the oligarchs have a constant semimajor axis for almost 100 Myr. When the total mass is a factor of two larger ( $\Sigma_l = 2 \text{ g cm}^{-2}$ ), the semimajor axes are constant for  $\sim 10^5 \text{ yr}$ . Once the orbits start to overlap, several oligarchs show considerable excursions in semimajor axis of 0.1 AU or more,  $\sim 30\%$  to  $40\%$  of the grid. Two of these oligarchs merge with other oligarchs. For  $\Sigma_l = 4 \text{ g cm}^{-2}$ , the orbits are very chaotic, with larger radial excursions and many mergers.

Figures 3 and 4 show the evolution of the number of oligarchs  $N_o$  and the orbit crossing parameter  $p_o$  for the three cases in Figures 1–2 and a fourth case with  $\Sigma_l = 8 \text{ g cm}^{-2}$ .

Mergers are prominent in all but the lower surface density test. In the tests where mergers are important,  $p_o \lesssim 0$  when orbits overlap and mergers begin.

These tests confirm our general expectations. Oligarchs stir up planetesimals along their orbits. Dynamical friction maintains a fixed ratio of  $e_l/e_s$  (equation 2). Because the dynamical friction timescale depends on the surface density, the orbits of oligarchs in more massive disks overlap on shorter timescales than the orbits of oligarchs in less massive disks. More massive disks contain more oligarchs, leading to more chaotic orbits on shorter timescales.

To provide additional tests, we consider two more sets of calculations. Models with fixed  $\Sigma_l$  and variable  $\Sigma_s$  gauge the importance of damping by leftover planetesimals. We first consider models with  $m_s = 10^{24}$  g and then examine calculations with  $m_s = 10^{16}$  g.

Figure 5 shows the evolution of semimajor axis for three calculations with  $\Sigma_s = 2 \text{ g cm}^{-2}$  (upper panel),  $\Sigma_s = 4 \text{ g cm}^{-2}$  (middle panel), and  $\Sigma_s = 8 \text{ g cm}^{-2}$  (lower panel). The tracks in the upper panel repeat those from the middle panel of Figure 2; chaos begins at  $\sim 10^5$  yr when the orbits start to overlap. As  $\Sigma_s$  increases, dynamical friction between the small and large objects is more efficient. The orbits overlap and chaos begins later when  $\Sigma_l/\Sigma_s \lesssim 0.5$ . The middle set of tracks in Figure 5 demonstrates this behavior: there is no chaos until the system has evolved for 1 Myr. However, in models where  $\Sigma_s$  exceeds  $\sim 8 \text{ g cm}^{-2}$ , viscous stirring among the planetesimals increases their velocity dispersions on shorter timescales. Larger viscous stirring results in larger orbital eccentricities for the oligarchs (equation 2) and a faster onset of chaos. For  $\Sigma_s = 8 \text{ g cm}^{-2}$ , orbits begin to overlap at  $\sim 3 \times 10^5$  yr. These chaotic interactions grow with  $\Sigma_s$ .

To test the importance of viscous stirring among planetesimals, Figure 6 repeats the calculations of Figure 5 for planetesimals with  $m_s = 10^{16}$  g. In this test, the ratio of orbital eccentricity is much larger,  $e_s/e_l \sim 75\text{--}80$ . The viscous stirring timescale for the planetesimals is much larger than 1 Myr. For all  $\Sigma_s = 4\text{--}32 \text{ g cm}^{-2}$ , planetesimal stirring is negligible. Because dynamical friction is important, the oligarchs remain well-separated and never develop overlapping orbits.

These tests demonstrate the main physical processes involved in the transition from oligarchy to chaos. Dynamical friction maintains a fixed ratio of  $e_l/e_s$  (equation 2). Viscous stirring increases the orbital eccentricities of planetesimals until the orbits of oligarchs interact. When large planetesimals contain a significant amount of mass, they contribute to the stirring. Otherwise, oligarchs provide all of the stirring. Once orbits overlap, chaos ensues. Chaos produces mergers and large excursions in semimajor axis, which starts the process that clears out the disk to produce large planets.

Three parameters –  $\Sigma_l/\Sigma_s$ ,  $p_H$ , and  $p_o$  – provide good measures of the transition from oligarchy to chaos. The Hill parameter measures when the oligarchs have enough mass to interact dynamically. The ratio  $\Sigma_l/\Sigma_s$  isolates the time when planetesimals cannot damp the oligarchs and thus prevent large-scale dynamical interactions. The orbit overlap parameter distinguishes times when orbit overlap is important.

To understand the transition from oligarchy to chaos in less idealized situations, we now consider complete planet formation simulations using the full hybrid code. The calculations start with 1–10 km planetesimals and allow all objects to collide, merge, and interact gravitationally. When objects in the coagulation code reach  $m \approx 2 \times 10^{25}$  ( $\Sigma_0/8$  g cm $^{-2}$ ) g, we promote them into the  $n$ -body code and follow their individual trajectories. We describe calculations in a small (large) torus in §3.3 (§3.4).

### 3.3. Planet formation at 0.86–1.14 AU

The calculations begin with 1–3 km planetesimals in a torus extending from 0.86 AU to 1.14 AU. We divide this region into 32 annuli and seed each annulus with planetesimals in nearly circular and coplanar orbits ( $e_0 = 10^{-5}$  and  $i_0 = e_0/2$ ). The planetesimals have surface density  $\Sigma = \Sigma_0(a/1 \text{ AU})^{-3/2}$ , with  $\Sigma_0 = 1\text{--}16$  g cm $^{-2}$  at 1 AU. In these calculations, we do not consider fragmentation, which generally speeds up the growth of the largest objects at the expense of mass loss from disruptions and gas drag (Wetherill & Stewart 1993; Kenyon & Luu 1998). Weidenschilling et al. (1997) consider a similar suite of calculations. Where it is possible to compare, our results agree with these calculations (see also Kominami & Ida 2002).

For  $\Sigma_0 = 8$  g cm $^{-2}$ , growth at 1 AU follows a standard pattern (Wetherill & Stewart 1993; Weidenschilling et al. 1997; Kenyon & Luu 1998). After a few thousand years, mergers produce a few large objects with radii of  $\sim 10$  km. As dynamical friction circularizes the orbits of these objects, runaway growth begins. It takes only  $10^4$  yr to produce several dozen 100–300 km objects. At  $\sim 2 \times 10^4$  yr, the first object is promoted into the  $n$ -body code. As larger objects form farther out in the disk, more promotions occur. These objects continue to grow rapidly until they reach ‘isolation’ masses of  $\sim 10^{26}$  g, when stirring begins to reduce gravitational focusing factors.

The transition to oligarchic growth begins at the inner edge of the grid and rapidly propagates outwards. At  $\sim 3 \times 10^5$  yr, the number of oligarchs with masses  $m \gtrsim 10^{26}$  g peaks at  $N_o \sim 7$ . Soon after oligarchic growth begins at the outer edge of the grid, oligarchs at the inner edge of the grid begin to interact dynamically. A wave of strong dynamical

interactions then moves out through the grid. It takes  $\sim 1$  Myr for the wave to move from  $\sim 0.85$  AU to  $\sim 1.15$  AU. During this period, some oligarchs merge. Others migrate through the grid on highly eccentricity orbits.

From  $\sim 1$  Myr onward, mergers slowly reduce  $N_o$ . It takes  $\sim 1$  Myr for the first 2 mergers and another  $\sim 2$  Myr for the second 2 mergers. After 100 Myr, only 3 oligarchs remain. One of these has  $m \sim 0.43 m_\oplus$ ,  $a \sim 0.9$  AU, and  $e \sim 0.08$ . The other two oligarchs have  $m \sim 0.05 m_\oplus$  and  $e \sim 0.1$  (Figure 7). Aside from the eccentricity of the more massive planet, the properties of these objects are reasonably close to those of the Earth and Mars. Fragmentation and interactions with the gas probably promote smaller eccentricities for the largest objects (e.g., Wetherill & Stewart 1993; Agnor & Ward 2002; Kominami & Ida 2002).

Figure 7 illustrates the evolution of the semimajor axes of the oligarchs for three calculations with  $\Sigma_0 = 2 \text{ g cm}^{-2}$  (lower panel),  $\Sigma_0 = 4 \text{ g cm}^{-2}$  (middle panel), and  $\Sigma_0 = 8 \text{ g cm}^{-2}$  (upper panel). As in Figure 1, the tracks change color when two oligarchs collide and merge. The labels indicate the final mass, in Earth masses, of the largest oligarchs at 100 Myr.

The timescale for the onset of chaotic growth depends on the initial surface density. More massive disks reach the transition first. (see, for example, Lissauer 1987). For  $\Sigma_0 = 8 \text{ g cm}^{-2}$ , the transition begins at  $\sim a \text{ few} \times 10^5 \text{ yr}$ . The transition is delayed to  $\sim 1$  Myr for  $\Sigma_0 = 2 \text{ g cm}^{-2}$ .

The character of the transition to chaotic growth also depends on the initial surface density. In relatively massive disks with  $\Sigma_0 \sim 8 \text{ g cm}^{-2}$ , many oligarchs develop highly eccentric orbits and exhibit large variations in their semimajor axes. These large excursions result in many mergers and a rapid reduction in  $N_o$ . In less massive disks with  $\Sigma_0 \lesssim 2\text{--}4 \text{ g cm}^{-2}$ , only 1 or 2 oligarchs develop highly eccentric orbits. Most mergers are caused by two-body interactions, instead of large-scale dynamical interactions throughout the grid.

Figures 8–10 illustrate these general conclusions. In Figure 8, the orbit crossing parameter rapidly approaches zero for calculations with  $\Sigma_0 = 8 \text{ g cm}^{-2}$ . At 0.1–1 Myr,  $p_o$  has a long plateau; close approaches between oligarchs cause  $p_o$  to fall below zero; mergers cause  $p_o$  to jump above zero. During a series of 4 mergers at 10 Myr,  $p_o$  remains below 0 for a long period. After the final merger,  $p_o$  jumps to 40, where it remains for many Myr. For smaller  $\Sigma_0$ ,  $p_o$  remains well above zero until one or two close pairwise interactions pushes it below zero. Once these interactions produce a merger, the systems stabilize and  $p_o$  moves well above zero.

Figure 9 shows the time evolution of the total number of  $n$ -bodies within the grid.

During the transition from runaway growth to oligarchic growth,  $N_o$  peaks and remains constant for 0.1–1 Myr. Once orbital interactions begin,  $N_o$  declines. The rate of decline is fastest in the most massive systems.

The Hill parameter also shows the rapid transition from oligarchy to chaos. When  $N_o$  peaks,  $p_H$  reaches a maximum. It declines sharply when mergers reduce the number of oligarchs. After a merger or series of mergers,  $p_H$  rises slowly as the remaining oligarchs accrete leftover planetesimals.

To examine the sensitivity of these results to  $m_{pro}$ , we consider a broad range of promotion mass. For  $\Sigma_0 = 1\text{--}16 \text{ g cm}^{-2}$  at 0.8–1.2 AU, calculations with  $m_{pro} \gtrsim 2 \times 10^{25} (\Sigma_0/4 \text{ g cm}^{-2}) \text{ g}$  cannot follow the evolution of the most massive coagulation particles accurately. Thus, the production rate of oligarchs is inconsistent. Once a few oligarchs form, the models provide a poor treatment of interactions among oligarchs and therefore yield poor estimates of the merger rate and the timescale for the transition from oligarchy to chaos.

Calculations with smaller  $m_{pro}$  provide better solutions to the evolution of the largest objects. To measure the quality of the results for the transition from oligarchy to chaos, we define  $t_\Sigma$  as the time when oligarchs with  $m \gtrsim 10^{26}(\Sigma_0/8 \text{ g cm}^{-2}) \text{ g}$  contain half of the initial mass and  $t_m$  as the time when these oligarchs start to merge and the number of oligarchs starts to decline. The scaling of the oligarch mass with  $\Sigma_0$  provides a clean way to compare models with different initial conditions.

Our calculations show clear trends for  $t_m$  and  $t_\Sigma$  as a function of  $\Sigma_0$  (Figure 11). The timescale for oligarchs to contain half of the initial mass roughly varies as  $t_\Sigma \propto \Sigma_0^{-2/3}$  with very little dispersion<sup>2</sup>. The transition from oligarchic growth to chaotic growth at  $t = t_m$  also depends on  $\Sigma_0$ . Our results yield an approximate relation,  $t_m \propto \Sigma_0^{-3/2}$ . However, this trend appears to have inflection points for  $\Sigma \lesssim 2 \text{ g cm}^{-2}$  and  $\Sigma \gtrsim 8 \text{ g cm}^{-2}$ . Calculations in progress will allow us to test this relation and its origin in more detail.

There are no large trends for  $t_m$  and  $t_\Sigma$  with  $m_{pro}$ . Although calculations with smaller  $m_{pro}$  yield smaller dispersions in  $t_m$  and  $t_\Sigma$  at each  $\Sigma_0$ , the median values for  $t_m$  and  $t_\Sigma$  are fairly independent of  $m_{pro}$ . A Spearman rank test (Press et al. 1992) suggests a weak inverse correlation between  $t_m$ ,  $t_\Sigma$  and  $m_{pro}$ , which we plan to test with additional calculations.

Independent of  $m_{pro}$ , our results demonstrate a clear trend of the ratio  $r_\Sigma = t_m/t_\Sigma$  with

---

<sup>2</sup>The origin of this relation lies in the growth and stirring rates. In the absence of stirring, the growth time is  $t \propto \Sigma_0^{-1}$ . Because more massive oligarchs form in more massive disks, the vertical scale height  $H$  of leftover planetesimals is larger in more massive disks. Larger scale heights reduce the growth rate by roughly  $H^{1/3} \propto \Sigma_0^{1/3}$ , which results in  $t_\Sigma \propto \Sigma_0^{-2/3}$ .

initial surface density (Table 1). In massive disks with  $\Sigma_0 \gtrsim 12 \text{ g cm}^{-2}$ , mergers among oligarchs begin before oligarchs contain half of the mass ( $t_m/t_\Sigma \lesssim 1$ ). In low mass disks with  $\Sigma_0 \lesssim 2 \text{ g cm}^{-2}$ , oligarchs start to merge after they contain half of the mass ( $t_m/t_\Sigma \gtrsim 1$ ).

To test whether variations in the frequency and strength of dynamical interactions among oligarchs cause the trends in  $t_m$  and  $r_\Sigma$ , we define a ‘nearest neighbor parameter’  $n_n$  which measures the average number of oligarchs within  $10 R_H$  of another oligarch. From §3.2, configurations with  $n_n \gtrsim 1$  lead to strong dynamical interactions among the oligarchs; oligarchs interact mildly when  $n_n \lesssim 1$ . Table 1 lists the average of the maximum value of  $n_n$  and its dispersion for our calculations. Disks with  $r_\Sigma \gtrsim 0.5$  have  $n_{n,max} \lesssim 1$ ; disks with  $r_\Sigma \lesssim 0.5$  have  $n_{n,max} \gtrsim 1$ . This result confirms the visual impressions from Figures 7–10: dynamical interactions among oligarchs are stronger in massive disks and milder in low mass disks.

To conclude this section, Figure 12 shows the evolution of the mass for each oligarch in one calculation. Here, points of one color correspond to the track of one oligarch. From  $\sim 10^4 \text{ yr}$  to  $\sim 10^5 \text{ yr}$ , large objects form and grow rapidly. Once stirring reduces gravitational focusing factors, growth slows. During the late stages of runaway growth and the early stages of oligarchic growth, several neighboring oligarchs merge. As their gravitational reach extends, these larger oligarchs grow faster and faster. Smaller oligarchs cannot compete for leftover planetesimals and grow slowly.

During chaotic growth, the largest oligarchs merge with smaller oligarchs. As the small oligarchs are depleted, the merger rate slows. With highly eccentric orbits, a few small oligarchs last for 10–30 Myr before colliding with a large oligarch. After 100 Myr, all but one small oligarch have collided and merged with the two large planets that remain at the end of the evolution.

### 3.4. Planet formation at 0.4–2 AU

These calculations begin with 5 km planetesimals in a torus extending from 0.4 AU to 2 AU. We divide this region into 40 annuli and seed each annulus with planetesimals in nearly circular and coplanar orbits ( $e_0 = 10^{-5}$  and  $i_0 = e_0/2$ ). To provide a contrast with previous simulations, the planetesimals have surface density  $\Sigma = \Sigma_0(a/1 \text{ AU})^{-1}$ , with  $\Sigma_0 = 2\text{--}16 \text{ g cm}^{-2}$  at 1 AU. Calculations with the more standard  $\Sigma \propto r^{-3/2}$  yield similar results. As in §3.3, we do not consider fragmentation. This torus is larger than the 0.5–1.5 AU region examined by Weidenschilling et al. (1997, see also Kominami & Ida 2002), but similar to the torus described by Chambers (2001). Chambers (2001) starts his calculations with lunar

mass objects, instead of planetesimals. Bromley & Kenyon (2006) compare results derived from our hybrid code for calculations starting with 1–10 km planetesimals or 100–200 lunar mass objects. When we start with smaller objects, our calculations produce fewer oligarchs on shorter timescales than the Chambers (2001) calculations.

Growth in the larger torus is similar to that in the smaller torus. For  $\Sigma_0 = 8 \text{ g cm}^{-2}$ , mergers produce a few large objects with radii of  $\sim 10 \text{ km}$  at 0.4 AU in roughly a thousand years. Once runaway growth begins, it takes only  $\sim 10^4 \text{ yr}$  for the first promotion into the  $n$ -body code. As runaway growth propagates outward in heliocentric distance, objects throughout the grid reach the isolation mass of  $\sim 10^{26} \text{ g}$ . It takes less than  $10^5 \text{ yr}$  to produce 10 isolated objects and another  $2 \times 10^5 \text{ yr}$  to produce the next 10 isolated objects. These objects continue to grow and reach typical masses of 0.05–0.1  $m_\oplus$  in  $\sim 1 \text{ Myr}$ .

During oligarchic growth, occasional two body interactions produce mergers of oligarchs. These mergers always occur when the coagulation code produces 2–3 oligarchs in the same annulus. Often, dynamical interactions move one or two oligarchs into neighboring annuli, where they begin to accrete planetesimals more rapidly. Occasionally, dynamical interactions between several oligarchs in neighboring annuli produce one or two mergers, which stabilizes the system locally and leads to the isolation of the remaining 2 or 3 oligarchs.

As oligarchs start to form at the outer edge of the grid, oligarchs at the inner edge of the grid begin to interact dynamically (Figure 12). For  $\Sigma_0 = 8 \text{ g cm}^{-2}$ , these interactions start at  $\sim 1 \text{ Myr}$ . Chaotic interactions then spread throughout the grid. For the next  $\sim 10 \text{ Myr}$ , mergers produce fewer but larger oligarchs, which rapidly sweep up the remaining planetesimals. After  $\sim 200 \text{ Myr}$ , only 5 oligarchs remain. The largest have masses comparable to those of the Earth and Venus. Smaller oligarchs have masses comparable to the mass of Mars.

As in §3.3, the evolution in less massive disks proceeds more slowly and less chaotically. The magnitude of dynamical orbital interactions is non-linear: once chaos starts in a massive disk, it rapidly propagates throughout the grid. Pairwise interactions dominate the dynamics of lower mass disks. These interactions usually do not affect other oligarchs.

Figures 13–14 show the time evolution of  $p_o$  and  $p_H$ . In all calculations, the typical orbital separation of the largest objects rapidly approaches zero when the first oligarchs form (Figure 13). This transition occurs sooner in more massive disks. During oligarchic growth, the orbits of oligarchs slowly move closer and closer. The number of oligarchs and the average Hill radius of the oligarchs (Figure 14) rise dramatically; these peak when  $\Sigma_l/\Sigma_s \sim 0.4$ –0.5. Once  $\Sigma_l/\Sigma_s \gtrsim 0.5$ , chaotic interactions cause oligarchs to merge. When the orbits overlap, large-scale chaos leads to rapid mergers and planets with masses comparable

to the mass of the Earth. In less massive disks with  $\Sigma_0 \lesssim 2 \text{ g cm}^{-2}$ , the oligarchs remain well-separated relative to their Hill radii (Figure 14). Pairwise interactions between oligarchs then produce most of the mergers. This evolution is slow and results in more planets with masses comparable to the mass of Mercury.

Finally, Figure 15 shows the growth of the oligarchs for a calculation with  $\Sigma_0 = 8 \text{ g cm}^{-2}$ . Here, tracks of a single color show the time evolution in the mass of a single oligarch. Tracks end when an oligarch merges with another oligarch in the grid.

The tracks in Figure 15 clearly illustrate the three stages of growth in the terrestrial zone. Most tracks are initially steep and then slowly turn over. The dramatic changes in the slope mark the transition from runaway growth to oligarchic growth. At  $\sim 10^5 \text{ yr}$ , this transition propagates as a wave from the inner part of the grid at 0.4 AU to the outer part of the grid at 2 AU.

The onset of distinct steps in mass indicates the transition from oligarchic growth to chaotic growth. Starting at  $\sim 1\text{--}3 \text{ Myr}$ , this transition takes  $\sim 3\text{--}10 \text{ Myr}$  to propagate from 0.4 AU to 2 AU. Once the full grid is chaotic, mergers rapidly separate the oligarchs into small oligarchs, with  $m \sim 0.01\text{--}0.1 m_\oplus$  and  $e \gtrsim 0.1$ , and large oligarchs, with  $m \gtrsim 0.2\text{--}1 m_\oplus$  and  $e \lesssim 0.05$ . After  $\sim 100 \text{ Myr}$ , this division is stark: there are 3 oligarchs with  $m \gtrsim 0.5 m_\oplus$  and 3 others with  $m \lesssim 0.07 m_\oplus$ .

Calculations with a large range in  $m_{pro}$  provide a measure of the quality of these conclusions. Because the 0.4–2 AU grid is much larger than the 0.84–1.16 AU grid, these calculations produce more oligarchs and are less sensitive to  $m_{pro}$  than calculations in a smaller grid. Nevertheless, calculations with  $m_{pro} \gtrsim 3 \times 10^{25} (\Sigma_0/4 \text{ g cm}^{-2}) \text{ g}$  yield a much larger range in the evolution timescales than calculations with smaller  $m_{pro}$ . As in §3.3, models with  $m_{pro} \sim 1 - 10 \times 10^{24} \text{ g}$  yield consistent results for these timescales.

### 3.5. Other Physics

In this set of calculations with the hybrid code, we concentrate on mergers and dynamical interactions between solid objects. We ignore fragmentation and interactions with the gas. In previous calculations, fragmentation of 1–10 km planetesimals produces cm- to m-sized fragments which are more closely coupled to the gas than larger planetesimals. Gas drag circularizes the orbits of these objects, which can then be accreted more rapidly than the leftover planetesimals. From previous numerical calculations, the onset of runaway and oligarchic growth are  $\sim 25\%$  sooner than illustrated in §3.3 and §3.4 (e.g., Wetherill & Stewart 1993; Kenyon & Luu 1999; Kenyon & Bromley 2004b, 2005).



Fragmentation is important for setting the visibility of the disk (Kenyon & Bromley 2004b). The rate of debris production from fragmentation typically peaks during the transition from runaway to oligarchic growth. If fragmentation produces an efficient collisional cascade, radiation pressure and Poynting-Robertson drag may eject small particles before the oligarchs can accrete the fragments. The disk then produces a substantial infrared excess (Kenyon & Bromley 2004b). If some process halts or slows the cascade, oligarchs can accrete the fragments efficiently (e.g., Goldreich, Lithwick & Sari 2004b). The disk may then produce a modest infrared excess. We have started calculations to evaluate the importance of fragmentation in setting the timescales for runaway and oligarchic growth and to estimate the amount of dusty debris as a function of time.

Interactions with the gas can produce significant evolution in the eccentricity and orbital semimajor axis of oligarchs (e.g., Artymowicz 1993; Agnor & Ward 2002; Kominami & Ida 2002; Tanaka, Takeuchi & Ward 2002; Tanaka & Ward 2004). In the calculations here, simple gas drag as in Adachi et al. (1976) has a negligible impact on the evolution of planetesimals and oligarchs. However, interactions with density waves can circularize the orbits of oligarchs on short timescales (e.g., Artymowicz 1993; Agnor & Ward 2002; Kominami & Ida 2002; Tanaka & Ward 2004) and can cause significant inward migration of the orbit (e.g. Artymowicz 1993; Tanaka, Takeuchi & Ward 2002). For a gaseous disk with the surface density of a minimum mass solar nebula, the circularization timescale for an oligarch is  $\tau_c \sim 0.1\text{--}0.2$  Myr at 1 AU (Agnor & Ward 2002; Tanaka & Ward 2004). Significant orbital migration of an oligarch can occur over  $\tau_m \sim 1\text{--}3$  Myr (Tanaka, Takeuchi & Ward 2002; Tanaka & Ward 2004). Thus, interactions with the gas occur on timescales comparable with timescales for oligarchs to grow and interact dynamically.

The estimates for orbital migration and eccentricity damping assume a large gas density in the disk. Observations of young stars suggest the dust – and presumably the gas – disappears in  $\sim 1\text{--}10$  Myr (e.g., Calvet et al. 2005; D’Alessio et al. 2005, and references therein). If the gas density declines exponentially with time as in equation (7) with  $t_0 \sim 1$  Myr, radial migration may have little impact on the evolution of oligarchs. Eccentricity damping, however, may play an important role in the transition from oligarchic to chaotic growth. We have begun calculations to see how eccentricity damping and radial migration change the outcomes of our calculations.

Together, fragmentation and interactions with the gas probably set the eccentricity of the final ensemble of planets. If fragmentation is efficient at converting intermediate mass objects into smaller fragments, the fragments can efficiently circularize the orbits of growing oligarchs (equation 2; Figures 5–6). Interactions with the gas also circularizes the orbits of the most massive objects. We have started a set of calculations to test the relative efficiency

of damping and fragmentation in setting the eccentricity of surviving oligarchs.

#### 4. SUMMARY

Our calculations with the hybrid  $n$ -body-coagulation code are the first to evolve an ensemble of planetesimals into a system of a few planets. The calculations reproduce both the standard results of coagulation calculations for the early stages of planet formation and the results of  $n$ -body calculations for the late stages of planet formation (see also Bromley & Kenyon 2006). In particular, we follow the evolution through the critical transition from oligarchic growth to chaotic growth, where objects evolve from isolated oligarchs into full-fledged planets. These calculations provide some new insights into the transition from oligarchic growth to chaotic growth (see also Kokubo & Ida 2002; Kominami & Ida 2002).

In a disk with initial surface density  $\Sigma_0 \gtrsim 3\text{--}16 \text{ g cm}^{-2}$  at 1 AU, collisions and mergers of 1–10 km planetesimals naturally lead to the formation of terrestrial planets with masses ranging from 0.05–2  $m_\oplus$  (see also Wetherill & Stewart 1993; Weidenschilling et al. 1997; Chambers 2001; Kokubo & Ida 2002, and references therein). The growth follows a standard pattern. Slow orderly growth rapidly gives way to runaway growth, which concentrates much of the initial mass into many protoplanets with masses  $\sim 10^{26} \text{ g}$ . Stirring of leftover planetesimals by the largest objects reduces gravitational focusing factors and slows growth. During oligarchic growth, large oligarchs become isolated and slowly accrete the leftovers.

Several factors produce a transition from oligarchic growth to chaotic growth (see also Kominami & Ida 2002). As the oligarchs grow, they contain an ever increasing fraction of the total mass. A few oligarchs merge but most remain isolated from other oligarchs. As their Hill radii grow, their orbits begin to overlap. When the surface density in oligarchs reaches a critical value, oligarchs interact chaotically. As gravitational interactions scatter oligarchs throughout the disk, the merger rate increases dramatically. Eventually only a few oligarchs remain in roughly circular orbits.

Our results isolate the two conditions necessary for the transition from oligarchy to chaos. When oligarchs contain roughly half of the mass of solid material in the disk,  $\Sigma_l \sim \Sigma_s$ , dynamical interactions between oligarchs are more important than dynamical friction from planetesimals (e.g., Goldreich, Lithwick & Sari 2004b). When the surface density in oligarchs exceeds a critical value,  $\Sigma_c \approx 2\text{--}3 \text{ g cm}^{-2}$ , oligarchs begin to interact chaotically (§3). More massive disks can reach this limit when  $\Sigma_l < \Sigma_s$  (Table 1). In less massive disks, milder dynamical interactions begin when  $\Sigma_l \gtrsim \Sigma_s$  (Figure 11). If the surface density in oligarchs remains below the critical value, interactions between oligarchs are less chaotic even when

$\Sigma_i \gtrsim \Sigma_s$ . Interactions among 2 or 3 oligarchs produce a small merger rate which eventually yields a system with lower mass planets compared to more massive disks.

Although dynamical interactions among the ensemble of oligarchs produce terrestrial mass planets in all disks, more massive disks yield more massive planets. Our results suggest a maximum mass,  $m_{max} \sim 1\text{--}2\ m_{\oplus}$  for  $\Sigma_0 \sim 8\text{--}16\ \text{g cm}^{-2}$  and  $m_{max} \sim 0.1\text{--}0.2\ m_{\oplus}$  for  $\Sigma_0 \sim 1\text{--}2\ \text{g cm}^{-2}$ . Because young stars appear to have a wide range of initial disk masses, we expect a wide range in the masses of terrestrial planets in exosolar systems. In future studies, we plan to address this issue in more detail.

In terrestrial planet formation, the transitions between different stages of growth produce distinct waves through the disk. During the transition from orderly growth to runaway growth, the increase in the collision rate rapidly propagates from the inner edge of the disk to the outer edge. This transition is rapid and takes  $\lesssim 10^5$  yr to move from 0.4 AU to 2 AU.

Although less rapid, the transitions from runaway to oligarchic growth and from oligarchic to chaotic growth also propagate from the inner disk to the outer disk. During the transition to chaotic growth, dynamical interactions tend to produce more chaotic orbits at the outer edge of the disk. This behavior depends on the surface density gradient. In disks with steep density gradients,  $\Sigma \sim \Sigma_0 a^{-n}$  with  $n \gtrsim 3/2$ , chaotic interactions propagate slowly outward. In disks with shallower density gradients,  $n \lesssim 1$ , dynamical interactions tend to concentrate more mass in the outer part of the disk. This difference in behavior is set by the growth rate,  $\sim P/\Sigma \sim a^{n+3/2}$ , where  $P$  is the orbital period: the wave of growth propagates more rapidly through disks with shallower density gradients (e.g. Lissauer 1987).

These results have several interesting consequences for the evolution of planets in the terrestrial zone (see also Kominami & Ida 2002). The transition from oligarchic to chaotic growth occurs on timescales,  $\sim$  a few Myr, well before radiometric evidence suggests the formation of the Earth was fairly complete (e.g., Yin et al. 2002). Planets are also fully formed well before the estimated time of the Late Heavy Bombardment,  $\sim 100\text{--}300$  Myr after the formation of the Sun (e.g., Tera, Papanastassiou, & Wasserburg 1974; Hartmann 1980; Ryder 2002; Koeberl 2003).

Throughout the chaotic growth phase, our calculations produce many lunar- to Mars-sized objects on highly eccentric orbits. These objects are good candidates for the ‘giant impactor’ that collided with the Earth to produce the Moon (Hartmann & Davis 1975; Cameron & Ward 1976; Benz, Slattery, & Cameron 1986; Canup 2004a,b). As we complete calculations with fragmentation and migration, predicted mass and eccentricity distributions for these objects will yield better estimates for the probability of these events.

Together with the dynamical influence of Jupiter (e.g., Kominami & Ida 2004), the

highly eccentric orbits of lower mass oligarchs have an important role in clearing the inner solar system (e.g., Goldreich, Lithwick & Sari 2004a; Kominami & Ida 2004) and delivering water to the Earth (Lunine et al. 2003). Traditionally, data from our solar system provide the only tests of clearing mechanisms (e.g., Grogan et al. 2001; Nesvorný et al. 2002a,b, and references therein). In the next decade, comparisons between predicted infrared excesses from the debris disks leftover from terrestrial planet formation and observations from *Spitzer* and *TPF-Darwin* will yield new constraints on clearing timescales and the evolution of volatile species in the terrestrial zone (e.g., Beichman et al. 2005). These comparisons will enable better numerical calculations and an improved understanding of the final stages of terrestrial planet formation.

We thank M. Geller and an anonymous referee for important comments that improved the content of this paper. We acknowledge a generous allotment,  $\sim 5$  cpu years, of computer time on the Silicon Graphics Origin-2000 computers ‘alhena’, ‘castor’, and ‘pollux’ and the Dell Linux cluster ‘cosmos’ at the Jet Propulsion Laboratory through funding from the JPL Institutional Computing and Information Services and the NASA Directorates of Aeronautics Research, Science, Exploration Systems, and Space Operations. We thank V. McGlasson, M. Phelps, and other staff members of the CfA computation facility for installation and support of the SUN cluster ‘hydra’, where we used  $\sim 6$  cpu years to perform many of our calculations. The *NASA Astrophysics Theory Program* supported part of this project through grant NAG5-13278.

## REFERENCES

- Adachi, I., Hayashi, C., & Nakazawa, K. 1976, *Progress of Theoretical Physics* 56, 1756
- Agnor, C. B., & Ward, W. R. 2002, *ApJ*, 567, 579
- Alexander, S. G., & Agnor, C. B. 1998, *Icarus*, 132, 113
- Artymowicz, P. 1993, *ApJ*, 419, 166
- Beichman, C. A., Bryden, G., Rieke, G. H., Stansberry, J. A., Trilling, D. E., Stapelfeldt, K. R., Werner, M. W., Engelbracht, C. W., Blaylock, M., Gordon, K. D., Chen, C. H., Su, K. Y. L., & Hines, D. C. 2005, *ApJ* preprint doi:10.1086/428115
- Benz, W., & Asphaug, E. 1999, *Icarus*, 142, 5
- Benz, W., Slattery, W. L., & Cameron, A. G. W. 1986, *Icarus*, 66, 515

- Bromley, B. C., & Kenyon, S. J. 2006, *AJ*, submitted
- Calvet, N., Briceño, C., Hernández, J., Hoyer, S., Hartmann, L., Sicilia-Aguilar, A., Megeath, S. T., D'Alessio, P. 2005, *AJ*, 129, 935
- Cameron, A. G. W., & Ward, W. R. 1976, In: , p. 120
- Canup, R. 2004a, *Icarus*, 168, 433
- Canup, R. 2004b, *ARA&A*, 42, 441
- Chambers, J. E. 2001, *Icarus*, 152, 205
- D'Alessio, P., Hartmann, L., Calvet, N., Franco-Hernández, R., Forrest, W. J., Sargent, B., Furlan, E., Uchida, K., Green, J. D., Watson, D. M., Chen, C. H., Kemper, F., Sloan, G. C., & Najita, J. 2005, *ApJ*, 621, 461
- Davis, D. R., Chapman, C. R., Weidenschilling, S. J., & Greenberg, R. 1985, *Icarus*, 62, 30
- Duncan, M. J., Levison, H. F., & Lee, M. H. 1998, *AJ*, 116, 2067
- Goldreich, P., Lithwick, Y., & Sari, R. 2004a, *ARA&A*, 42, 549
- Goldreich, P., Lithwick, Y., & Sari, R. 2004b, *ApJ*, 614, 497
- Greenberg, R., Wacker, J. F., Hartmann, W. K., & Chapman, C. R. 1978, *Icarus*, 35, 1
- Greenberg, R., Weidenschilling, S. J., Chapman, C. R., & Davis, D. R. 1984, *Icarus*, 59, 87
- Greenzweig, Y., & Lissauer, J. J. 1990, *Icarus*, 87, 40
- Grogan, K., Dermott, S. F., & Durda, D. D. 2001, *Icarus*, 152, 251
- Haisch, K., Lada, E. A., & Lada, C. J. 2001, *ApJ*, 553, 153
- Hartmann, W. K. 1980, In *Conference on the Lunar Highlands Crust*, edited by J. Papike & R. Merrill, Pergamon, New York, p. 155
- Hartmann, W. K., & Davis, D. R. 1975, *Icarus*, 24, 504
- Hayashi, C. 1981, *Prog Theor Phys Suppl*, 70, 35
- Ida, S., & Makino, J. 1993, *Icarus*, 106, 210
- Kenyon, S. J., & Bromley, B. C., 2002, *ApJ*, 577, L35

- Kenyon, S. J., & Bromley, B. C., 2004a, AJ, 128, 1916
- Kenyon, S. J., & Bromley, B. C., 2004b, ApJ, 602, L133
- Kenyon, S. J., & Bromley, B. C., 2005, AJ, submitted
- Kenyon, S. J., & Hartmann, L. 1987, ApJ, 323, 714
- Kenyon, S. J., & Luu, J. X. 1998, AJ, 115, 2136
- Kenyon, S. J., & Luu, J. X. 1999, AJ, 118, 1101
- Koeberl, C. 2003, EM&P, 92, 79
- Kokubo, E., & Ida, S. 1995, Icarus, 114, 247
- Kokubo, E., & Ida, S. 1996, Icarus, 123, 180
- Kokubo, E., & Ida, S. 1998, Icarus, 131, 171
- Kokubo, E., & Ida, S. 2000, Icarus, 143, 15
- Kokubo, E., & Ida, S. 2002, ApJ, 581, 666
- Kominami, J. & Ida, S. 2002, Icarus, 157, 43
- Kominami, J. & Ida, S. 2004, Icarus, 167, 231
- Lissauer, J. J. 1987, Icarus, 69, 249
- Lissauer, J. J., & Stewart, G. R. 1993, In *Protostars and Planets III*, edited by E. H. Levy and J. I. Lunine, U. of Arizona Press, Tucson, 1061
- Lunine, J. I., Chambers, J., Morbidelli, A., & Leshin, L. A. 2003, Icarus, 165, 1
- Nesvorný, D., Bottke, W. F., Dones, L., & Levison, H. F. 2002a, Nature, 417, 720
- Nesvorný, D., Morbidelli, A., Vokrouhlický, D., Bottke, W. F., & Brož, M. 2002b, Icarus, 157, 155
- Ohtsuki, K., Stewart, G. R., & Ida, S. 2002, Icarus, 155, 436
- Press, W. H., Flannery, B. P., Teukolsky, S. A., & Vetterling, W. T. 1992, *Numerical Recipes, The Art of Scientific Computing*, Cambridge, Cambridge
- Rafikov, R. R. 2001, AJ, 122, 2713

- Rafikov, R. R. 2003a, AJ, 125, 906
- Rafikov, R. R. 2003b, AJ, 125, 922
- Rafikov, R. R. 2003c, AJ, 125, 942
- Rafikov, R. R. 2003d, AJ, 126, 2529
- Ryder, G. 2002, J. Geophys. Res., 107, E4, 6-1
- Safronov, V. S. 1969, *Evolution of the Protoplanetary Cloud and Formation of the Earth and Planets*, Nauka, Moscow [Translation 1972, NASA TT F-677]
- Spaute, D., Weidenschilling, S. J., Davis, D. R., & Marzari, F. 1991, Icarus, 92, 147
- Tanaka, H., Takeuchi, T., & Ward, W. R. 2002, ApJ, 565, 1257
- Tanaka, H., & Ward, W. R. 2004, ApJ, 602, 388
- Tera, F., Papanastassiou, D. A., & Wasserburg, G. J. 1974, Earth Planet. Sci. Lett., 22, 1
- Thommes, E. W., Duncan, M. J., & Levison, H. F. 2002, AJ, 123, 2862
- Thommes, E. W., Duncan, M. J., & Levison, H. F. 2003, Icarus, 161, 431
- Weidenschilling, S. J. 1977, Astrophys Sp Sci, 51, 153
- Weidenschilling, S. J., Spaute, D., Davis, D. R., Marzari, F., & Ohtsuki, K. 1997, Icarus, 128, 429
- Wetherill, G. W., & Stewart, G. R. 1989, Icarus, 77, 300
- Wetherill, G. W., & Stewart, G. R. 1993, Icarus, 106, 190
- Yin, Q., Jacobsen, S. B., Yamashita, K., Blichert-Toft, J., & Télouk, P., & Albarède, F. 2002, Nature, 418, 949
- Young, E. T., et al. 2004, ApJS, 154, 428

Table 1. Transition from Oligarchy to Chaos at 0.84–1.16 AU

$\Sigma_0$ (g cm <sup>-2</sup> )	$\log t_m$ (yr)	$r_\Sigma$	$n_{n,max}$
1	$7.0 \pm 0.05$	$0.58 \pm 0.01$	$0.85 \pm 0.05$
2	$6.6 \pm 0.05$	$0.53 \pm 0.01$	$0.91 \pm 0.05$
4	$6.3 \pm 0.07$	$0.48 \pm 0.02$	$0.99 \pm 0.10$
8	$6.0 \pm 0.08$	$0.41 \pm 0.02$	$1.11 \pm 0.07$
12	$5.7 \pm 0.10$	$0.32 \pm 0.03$	$1.24 \pm 0.12$
16	$5.3 \pm 0.10$	$0.24 \pm 0.03$	$1.33 \pm 0.11$



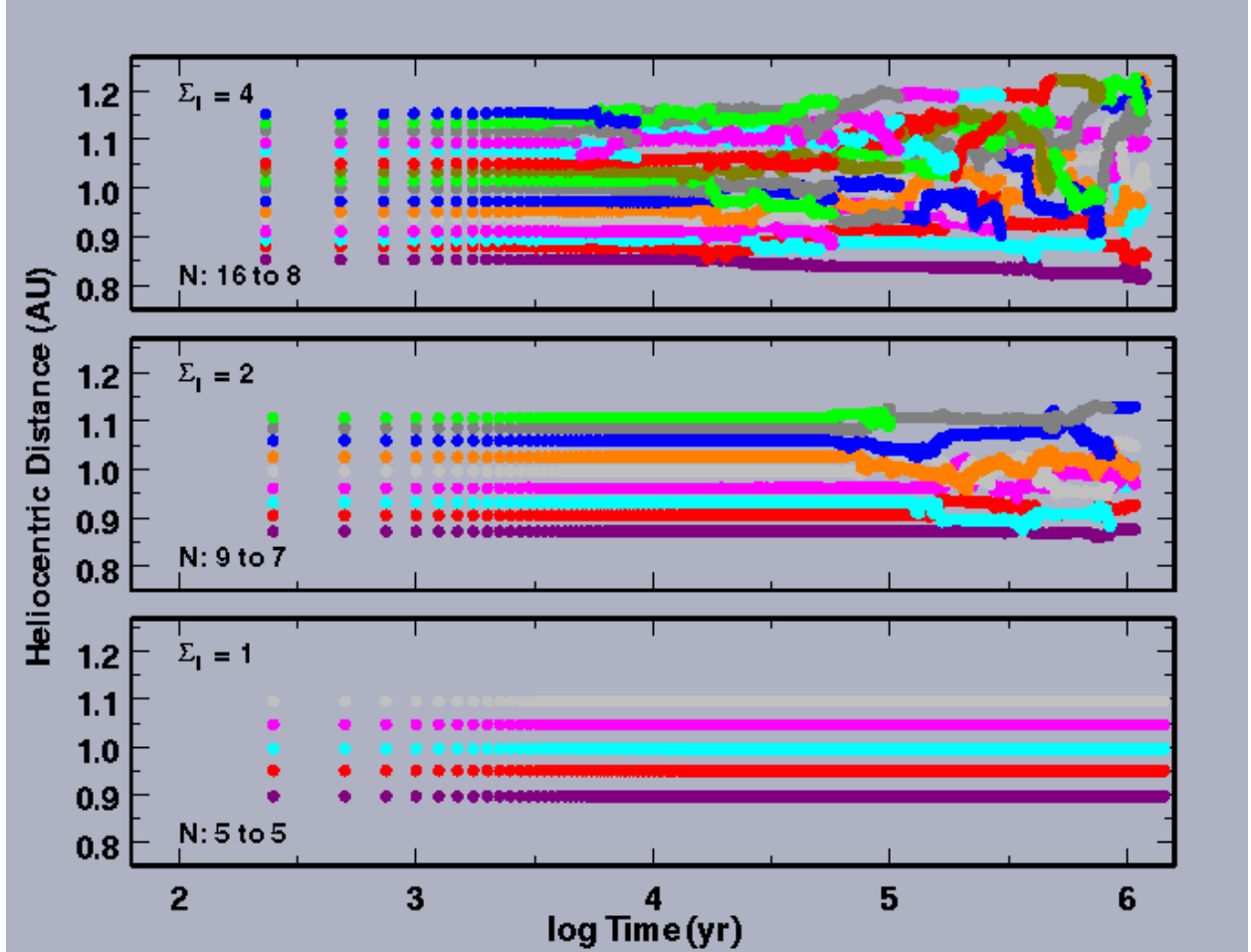


Fig. 1.— Evolution of eccentricity for oligarchs in a swarm of lower mass planetesimals. Each colored track shows the eccentricity of a single oligarch with time. A change in the color of a track (for example, in the middle panel at 1 Myr when the dark gray track turns blue) indicates a merger of one pair of oligarchs. The legend of each panel lists the surface density  $\Sigma_l$  in  $\text{g cm}^{-2}$  at 1 AU of oligarchs with individual masses  $m_s = 10^{26}$  g. In each panel, the surface density  $\Sigma_s$  of planetesimals with masses  $m_s = 10^{24}$  g equals the surface density of oligarchs. When  $\Sigma_l \lesssim 1 \text{ g cm}^{-2}$ , the orbits of oligarchs do not overlap on timescales of 1 Myr. For  $\Sigma_l \gtrsim 2 \text{ g cm}^{-2}$ , gravitational stirring leads to overlapping orbits and mergers of oligarchs. More massive systems develop overlapping orbits on shorter timescales, which leads to more mergers on timescales of 1 Myr or less.

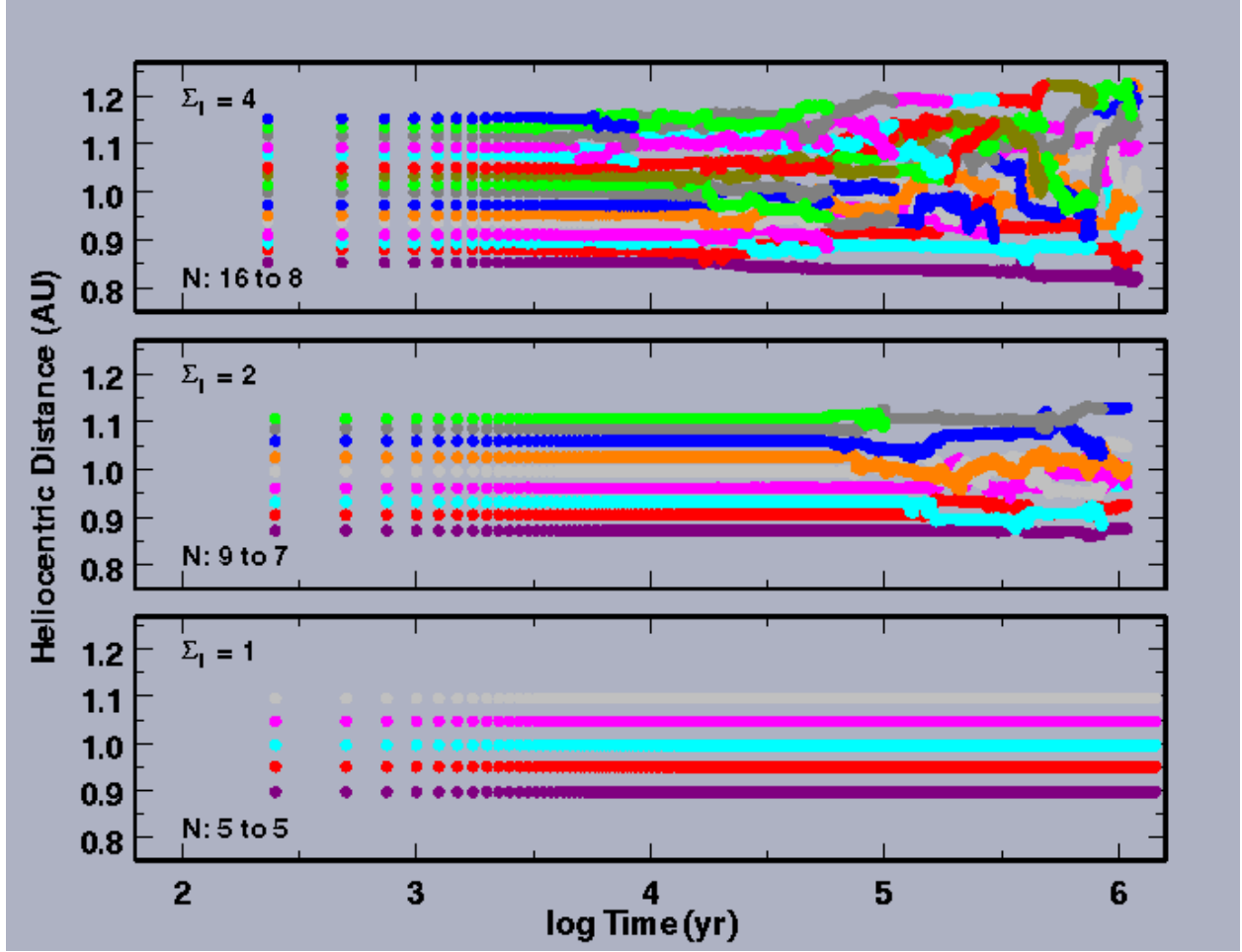


Fig. 2.— As in Figure 1 for the semimajor axes of the oligarchs. The legend in the lower left corner of each panel indicates the number of oligarchs at the beginning and end of each calculation.

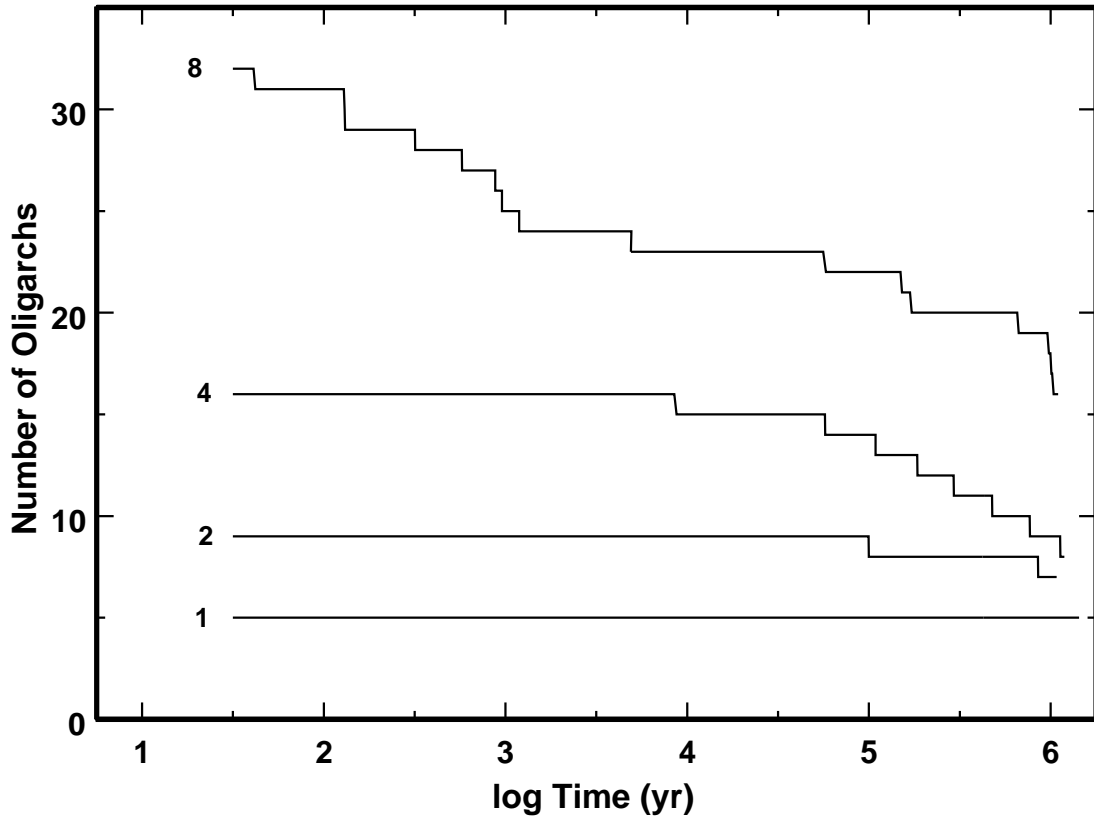


Fig. 3.— Evolution of the number of oligarchs for models with  $\Sigma_l = 1\text{--}8 \text{ g cm}^{-2}$ . More massive systems produce more mergers on shorter timescales.

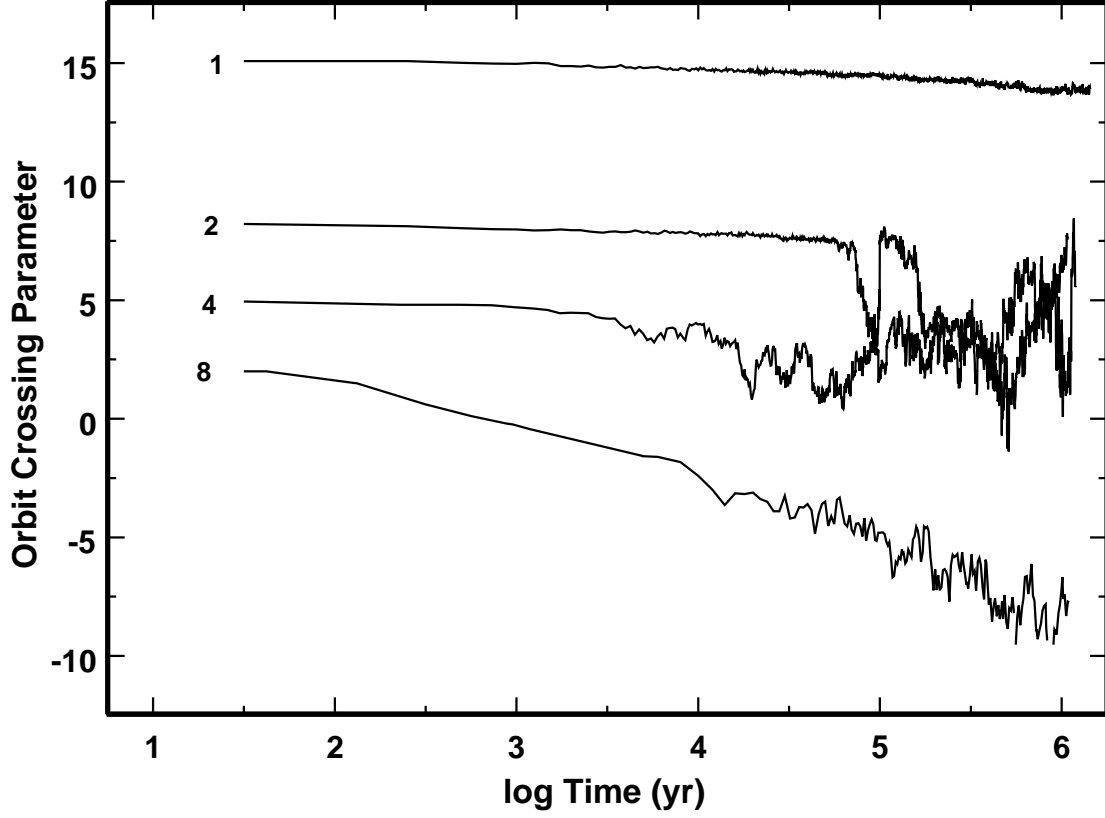


Fig. 4.— Evolution of the orbit crossing parameter  $p_o$  for models with  $\Sigma_l = 1\text{--}8 \text{ g cm}^{-2}$ . For  $p_o \gtrsim 2$ , orbits of oligarchs do not overlap and mergers do not occur. As  $p_o$  approaches 0, overlapping orbits of larger objects lead to mergers.

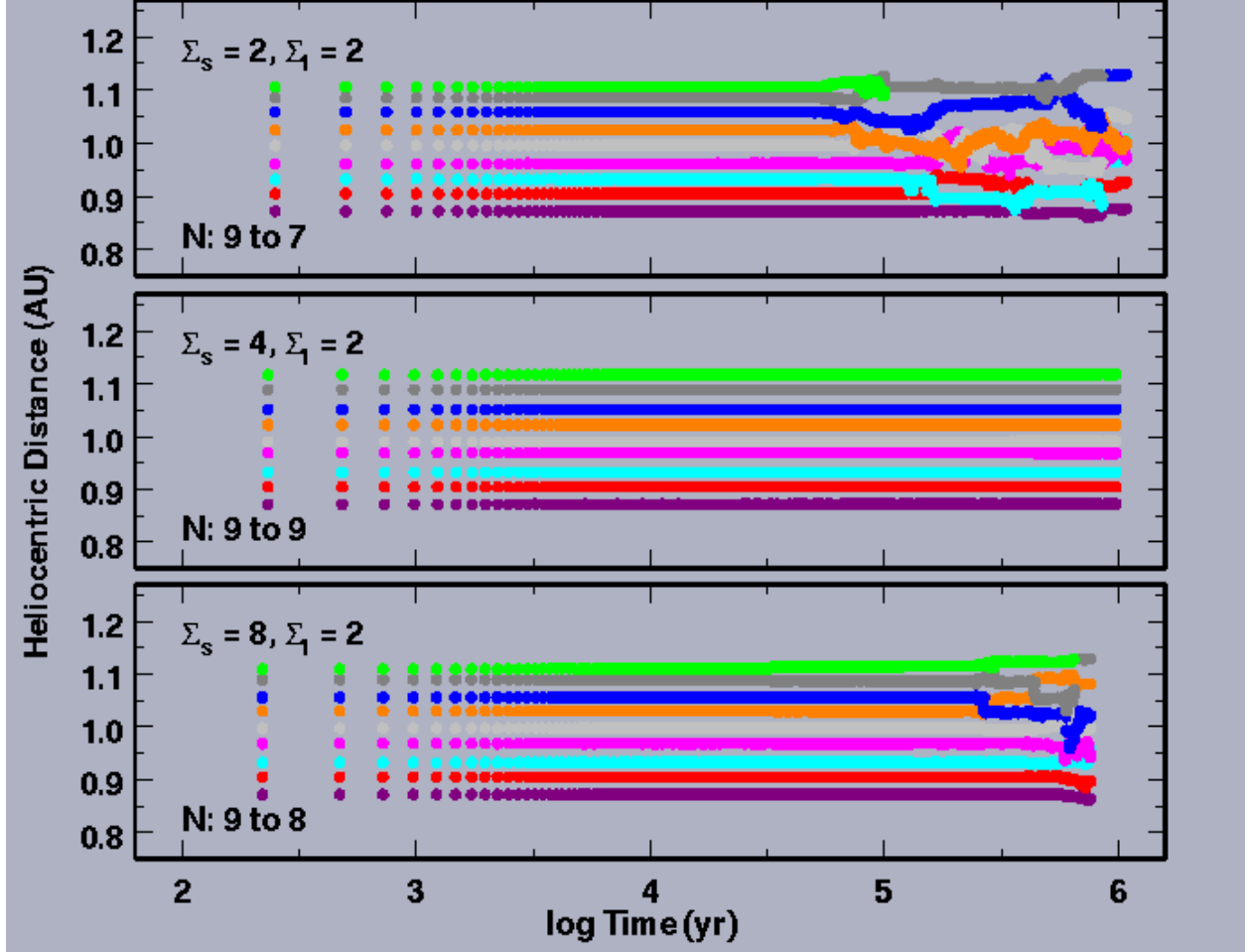


Fig. 5.— Evolution of semimajor axes for oligarchs in a swarm of lower mass planetesimals. As in Figure 1, each colored track show the position of one oligarch; changes in color along a track indicate a merger. The legend of each panel lists the number of oligarchs and the surface densities of planetesimals with  $m_s = 10^{24}$  g ( $\Sigma_s$ ) and oligarchs with  $m_l = 10^{26}$  g ( $\Sigma_l$ ) at 1 AU. As more mass is placed in smaller objects, dynamical friction first reduces orbit overlap between oligarchs. However, when the planetesimals contain more mass, viscous stirring between planetesimals aids orbit overlap and leads to mergers of the oligarchs.

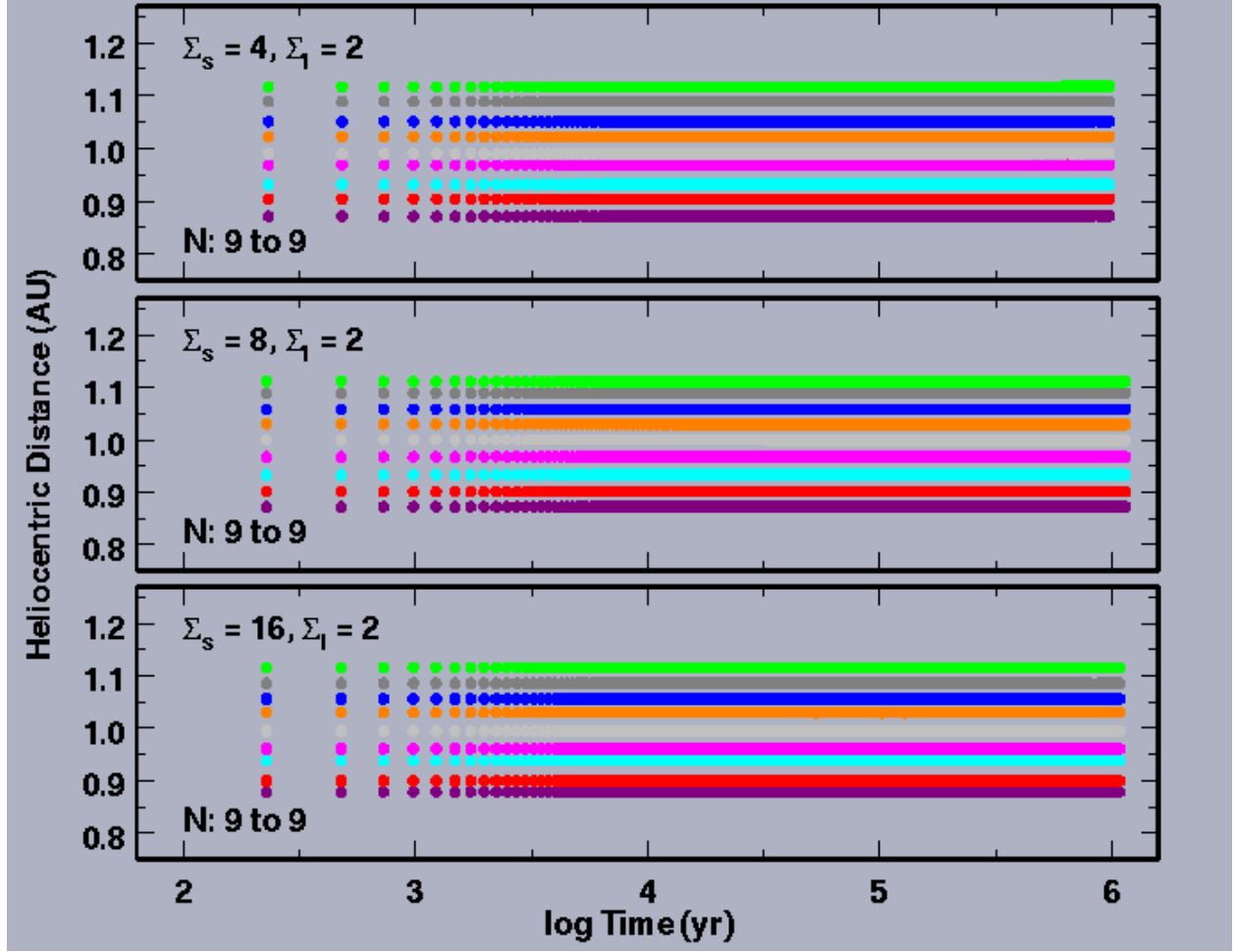


Fig. 6.— As in Figure 4 for  $m_s = 10^{16}$  g. Viscous stirring between planetesimals is minimal and does not lead to overlapping orbits of oligarchs in 1 Myr.

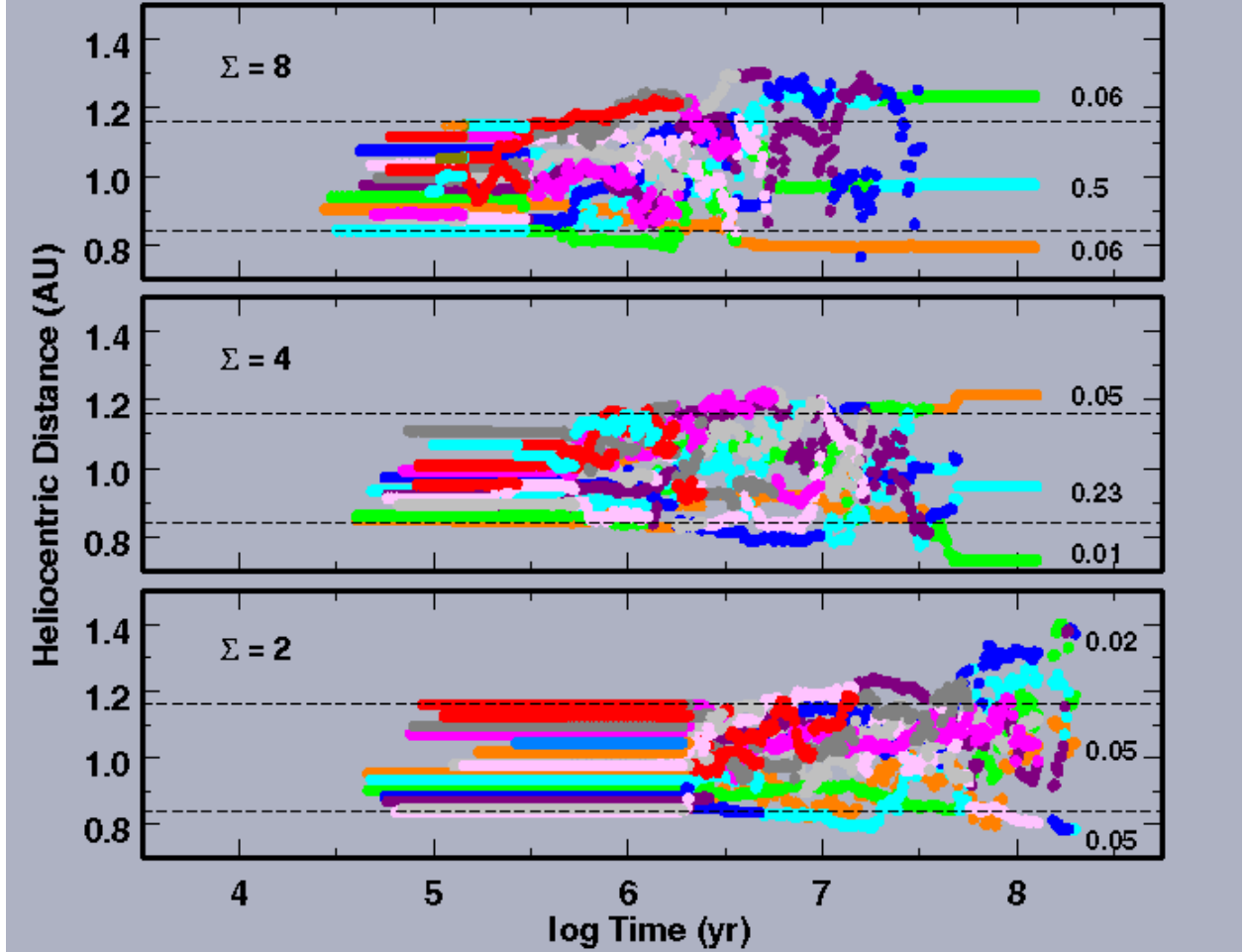


Fig. 7.— Evolution of semimajor axes for oligarchs with masses larger than  $m_{pro} = 10^{25}$  ( $\Sigma_0/4 \text{ g cm}^{-2}$ ) g in a full planet formation calculation at 0.86–1.14 AU. The legend of each panel lists the initial surface density in 1–10 km planetesimals at 1 AU (upper left corner, in units of  $\text{g cm}^{-2}$ ), and the mass of the largest planets (in  $m_\oplus$ ; at the right end of each track). The dashed lines indicate the extent of the planetesimal grid in the coagulation code. Runaway growth produces protoplanets in  $10^4$  yr to  $10^5$  yr. Continued growth of protoplanets during the oligarchic phase leads to orbit overlap on timescales of roughly 1 Myr. More massive systems reach this limit faster than less massive systems. Overlapping orbits leads to merger and more rapid growth of protoplanets.

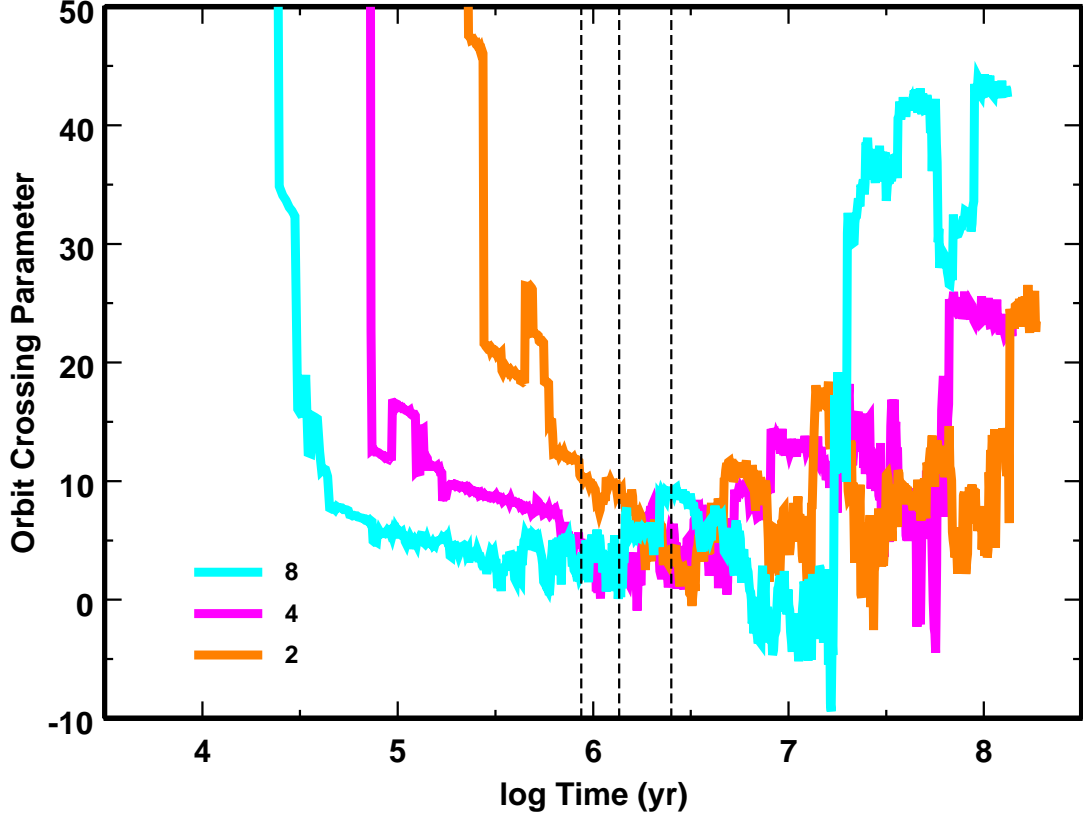


Fig. 8.— Evolution of the orbit crossing parameter  $p_o$  for the models of Figure 7. The legend lists the surface density in units of  $\text{g cm}^{-2}$  for each model. The dashed lines indicate when the surface density of oligarchs is half the total surface density. The leftmost dashed line corresponds to the largest initial surface density; the rightmost line corresponds to the smallest initial surface density. As oligarchs form,  $p_o$  declines and reaches a plateau where  $p_o \approx 1\text{--}5$ . Continued growth of the oligarchs leads to a minimum in  $p_o$ , roughly when  $\Sigma_l \approx \Sigma_s$ . minima Subsequent mergers reduce  $p_o$  until the system is in rough equilibrium, when  $p_o$  increases dramatically.



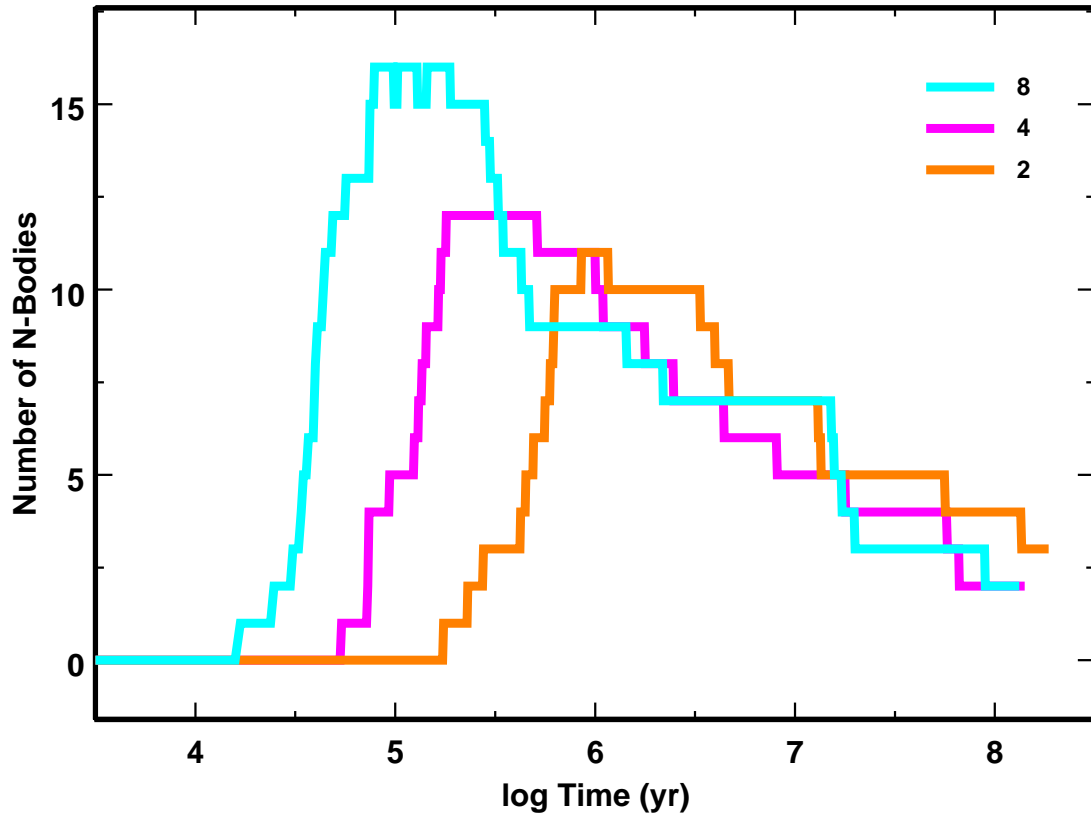


Fig. 9.— Evolution of the number of oligarchs  $N_o$  for the models of Figure 7.

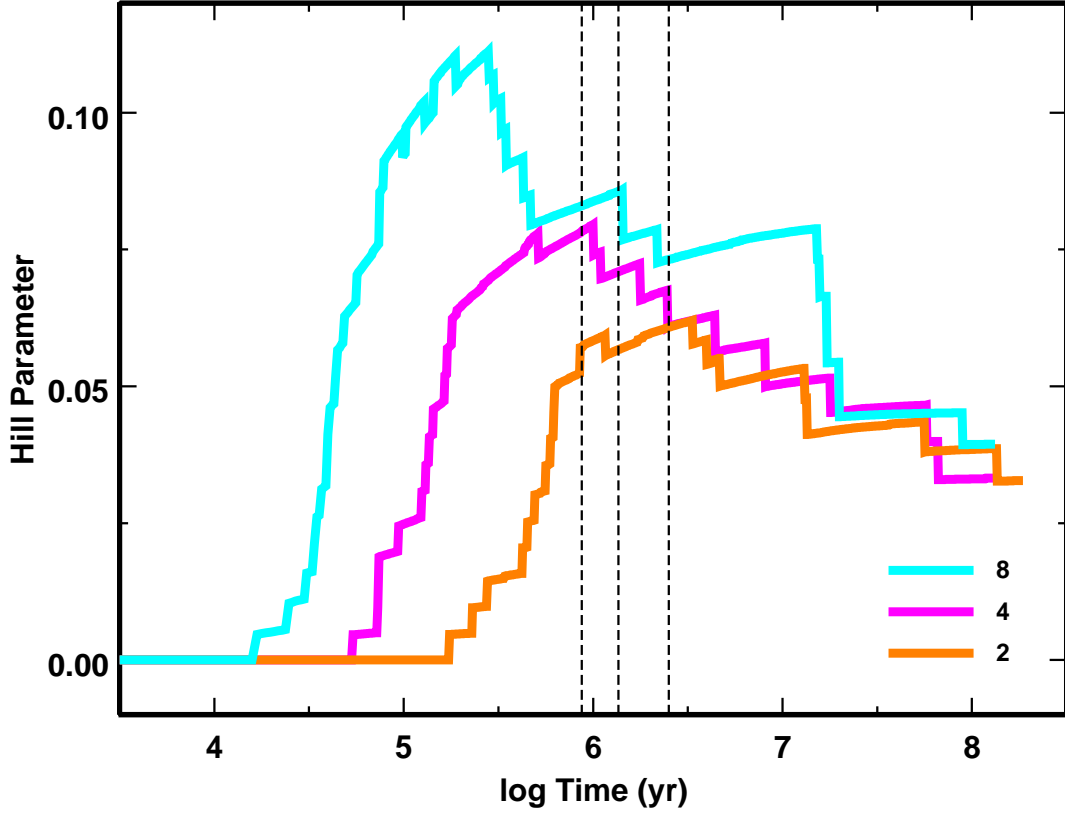


Fig. 10.— Evolution of the Hill parameter  $p_H$  for the models of Figure 7. The dashed lines indicate when the surface density of oligarchs is half the total surface density. The leftmost dashed line corresponds to the largest initial surface density; the rightmost line corresponds to the smallest initial surface density. When the number of oligarchs is maximum, the Hill parameter peaks. Mergers reduce  $p_H$ ; growth increases  $p_H$ . Chaotic growth occurs when  $p_H \gtrsim 0.07$ – $0.1$ .

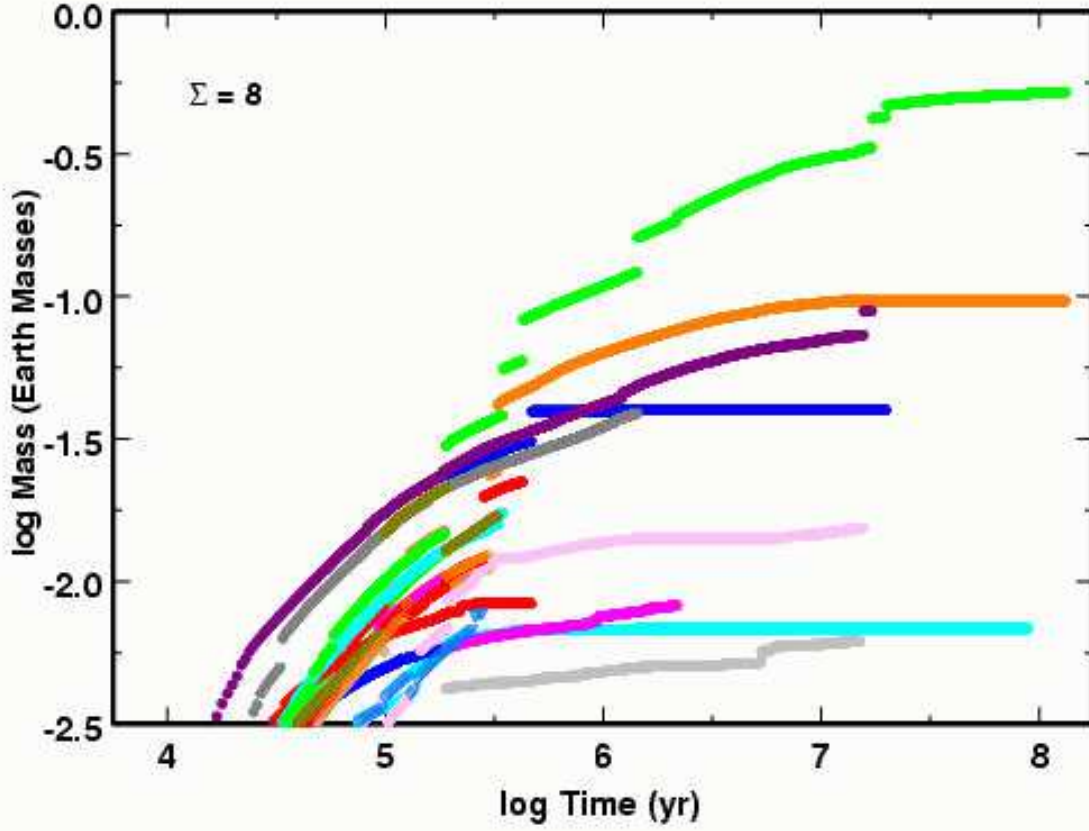


Fig. 11.— Variation of  $t_\Sigma$  and  $t_m$  as a function of  $\Sigma_0$  for different values of  $m_{pro}$ . The legend indicates symbols for the logarithm of the promotion mass. For each promotion mass and surface density, the points indicate typical values and extreme values. Thus, the two panels provide a visual impression of the dispersion of the results among a large set of calculations.

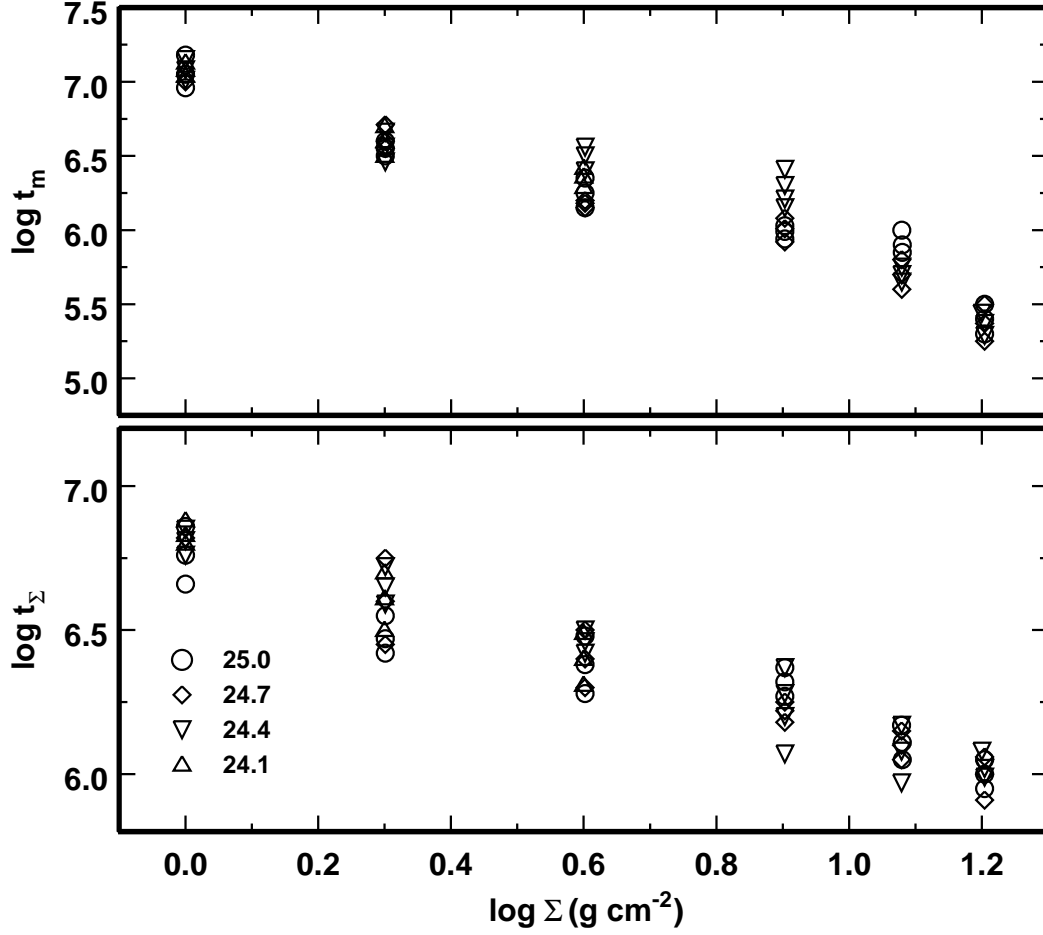


Fig. 12.— Evolution of masses for oligarchs with masses larger than  $2 \times 10^{25}$  g in a full planet formation calculation at 0.86–1.14 AU. The legend lists the initial surface density in 1–10 km planetesimals at 1 AU (upper left corner, in units of  $\text{g cm}^{-2}$ ). Each colored track shows the mass evolution for one oligarch. Discontinuities or terminations in the tracks indicate mergers of large objects.

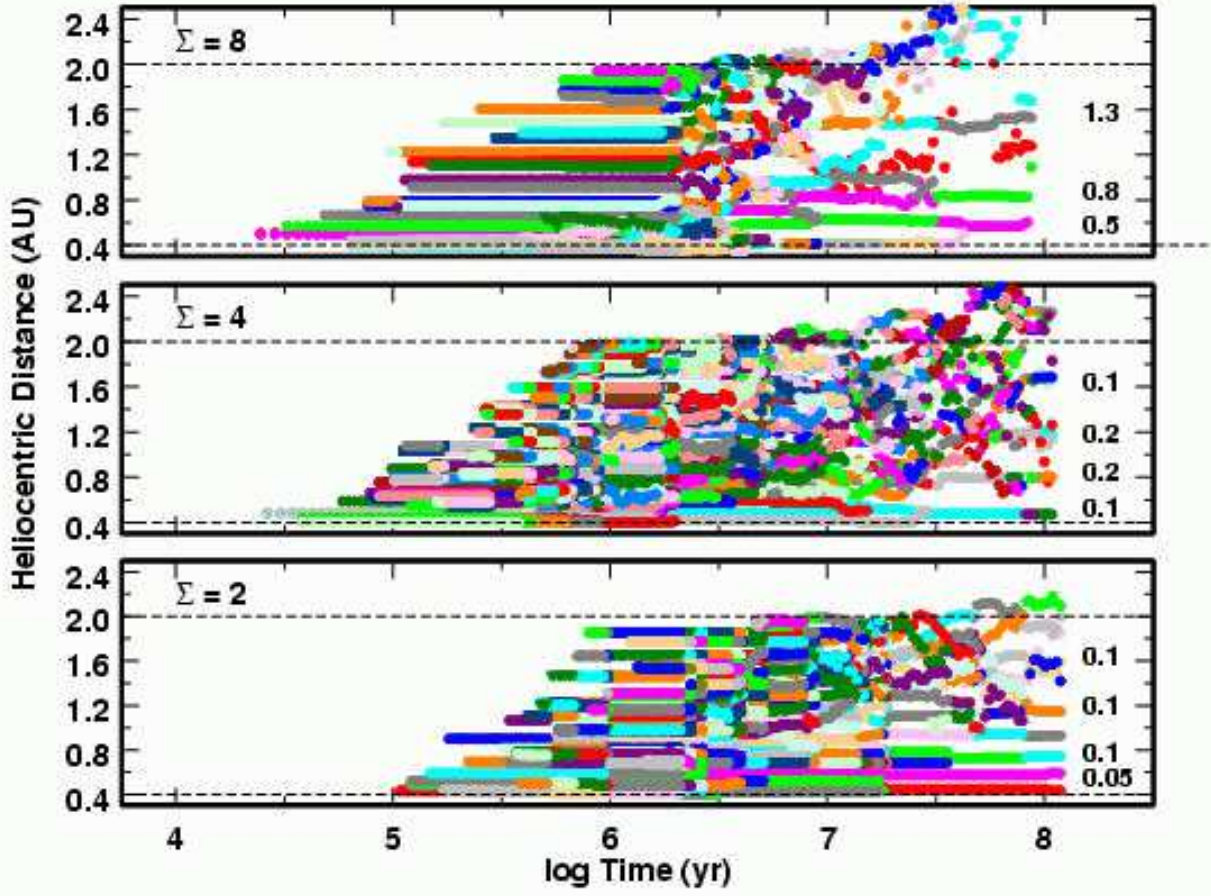


Fig. 13.— As in Figure 7 for a calculation at 0.4–2 AU with  $m_{pro} = 2 \times 10^{25} (\Sigma/4 \text{ g cm}^{-2}) \text{ g}$ .

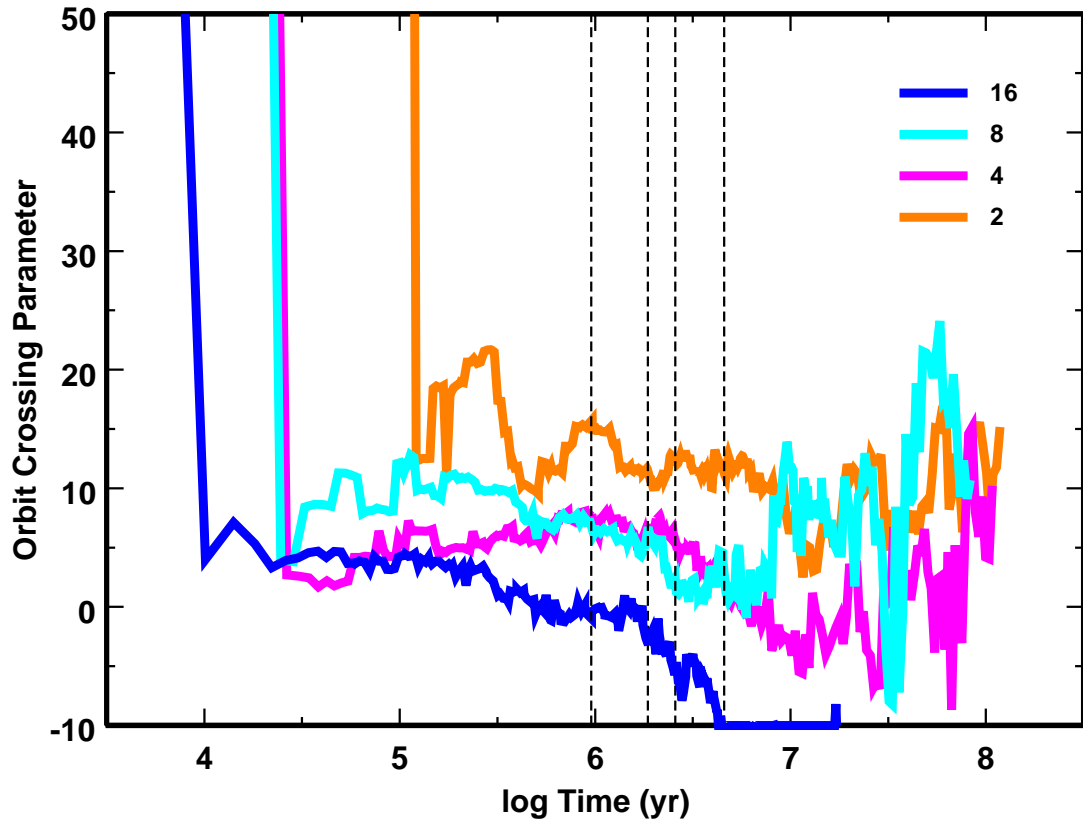


Fig. 14.— As in Figure 8 for the models of Figure 13.

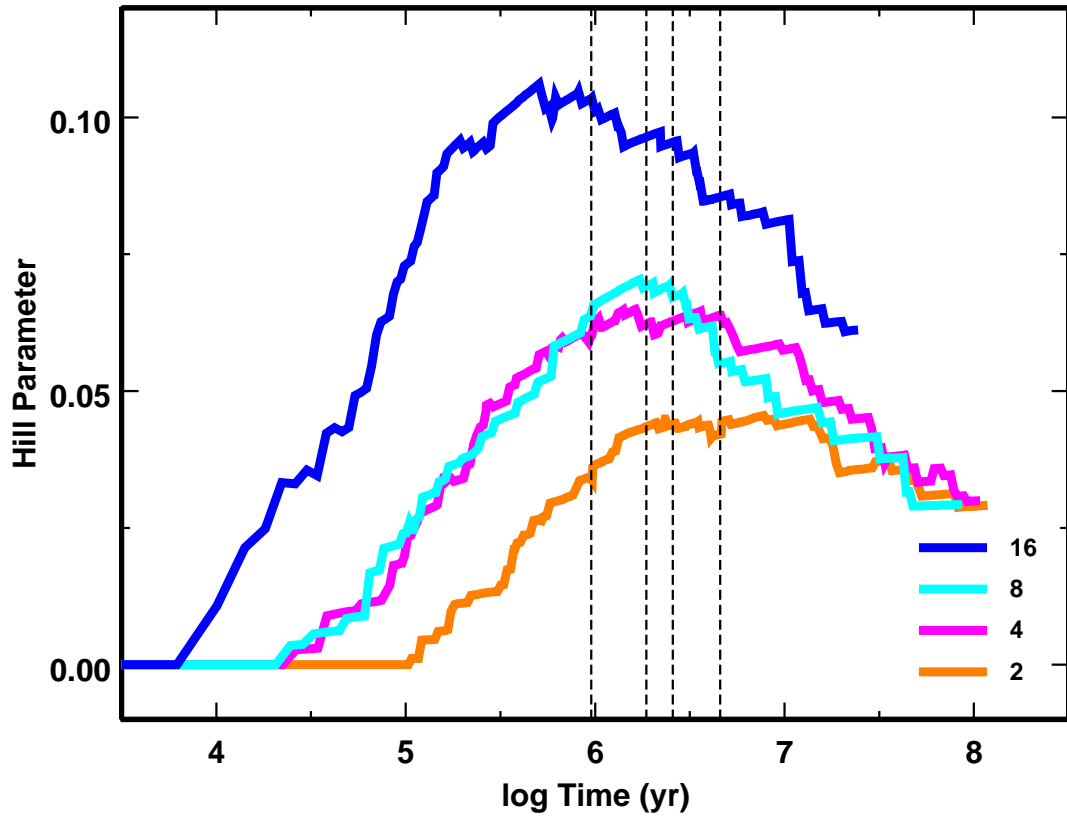


Fig. 15.— As in Figure 10 for the models of Figure 13.

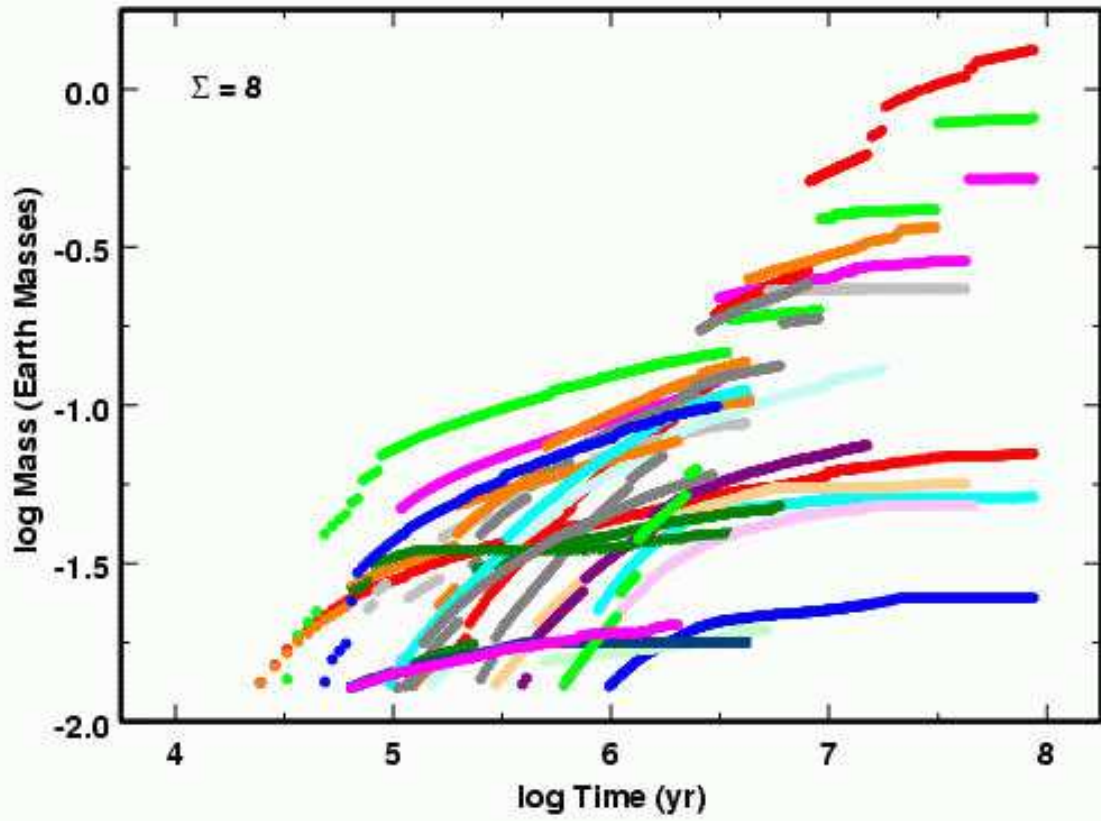


Fig. 16.— As in Figure 12 for a model from Figure 13.